© 2021. Published by The Company of Biologists Ltd | Journal of Cell Science (2021) 134, jcs258802. doi:10.1242/jcs.258802

RESEARCH ARTICLE

Plekhh1, a partner of myosin 1 and an effector of EphB2, controls the cortical actin network during cell repulsion

Marie-Thérèse Prospéri[1,2], Julien Pernier[2,3], Hugo Lachuer[1,2] and Evelyne Coudrier[1,2,*]

ABSTRACT

EphB2–ephrinB signalling, which plays a major role in cell segregation during embryonic development and tissue homeostasis, induces an important reorganization of the cortical actin network. We have previously reported that myosin 1b contributes to reorganization of the cortical actin network upon EphB2 signalling. In this report, we identify Plekhh1 as a new partner of members of the myosin 1 family and EphB2 receptors. Plekhh1 interacts with myosin 1b via its N-terminal domain and with EphB2 via its C-terminal domain. Furthermore, Plekhh1 is tyrosine phosphorylated, and this depends on EphB2 kinase activity. Similar to the effects of manipulating levels of myosin 1b and myosin 1c, manipulation of Plekhh1 expression levels alters the formation of filopodia, the length of focal adhesions and the formation of blebs. Furthermore, binding of the Plekhh1 interacting domain to myosin 1b increases the motor activity of myosin 1b *in vitro*. Taken together, our data show that Plekhh1 is an effector of EphB2 and suggest that Plekhh1 regulates the cortical actin network via the interaction of its N-terminal domain with myosin 1 upon EphB2–ephrinB signalling.

KEY WORDS: Myosin 1, Actin, EphB2, EphrinB, EphB2–EphrinB signalling, Cell repulsion

INTRODUCTION

The formation and maintenance of sharp borders between adjacent cell populations with different functions has a crucial role in the establishment and homeostasis of tissues during development and in adulthood (Batlle and Wilkinson, 2012; Fagotto et al., 2013). Current evidence suggests a model whereby the separation between different cell populations is controlled by cell surface cues such as pairs of ligands and receptors. Ligand–receptor signalling generates important changes in the cortical actin cytoskeleton, leading to modifications in cell protrusions, cell polarity, adhesion and the contractile actomyosin network (Batlle and Wilkinson, 2012; Klein, 2012; O'Neill et al., 2016). The EphB subclass of erythropoietin-producing hepatoma-amplified sequence (Eph) receptors are a large family of transmembrane tyrosine kinase receptors that are widely expressed in vertebrate tissues. They interact with ephrinB ligands, which are also transmembrane proteins, and play a major role in establishing and maintaining tissue organization (Batlle et al., 2002; Klein, 2012; Rohani et al., 2011). Restricted cell migration mediated by the activation of EphB receptors involves significant changes in cell morphology, including cell contraction and formation of cell protrusions as well as remodelling of the actin cytoskeleton (Groeger and Nobes, 2007; Kayser et al., 2008; Marston et al., 2003; Moeller et al., 2006; Prospéri et al., 2015; Zimmer et al., 2003). We have previously reported that myosin 1b (Myo1b) acts as an effector of the EphB2 receptor for cell repulsion (Prospéri et al., 2015). Myosin 1b regulates the formation of actomyosin fibres and filopodia at the interface of ephrinB1- and EphB2-expressing cells – two processes mediated by EphB2 signalling that contribute to cell repulsion (Prospéri et al., 2015).

The first members of the myosin 1 family were discovered in amoebae, but myosin 1 proteins are widely expressed. Myosin 1 proteins contain a motor domain at their N terminus, which binds to F-actin in response to ATP hydrolysis, a light chain-binding domain (LCBD), which binds to calmodulin (in most cases), and a tail domain at the C terminus (McIntosh and Ostap, 2016). The tail domain encompasses a tail homology domain (TH1) and a pleckstrin homology (PH) motif that binds to phosphoinositides. Eight isoforms (Myo1a–Myo1h) are found in higher vertebrates (McIntosh and Ostap, 2016), and these are classified as either short-tail myosin 1 proteins (Myo1a–Myo1d, Myo1g and Myo1h) or long-tail myosin 1 proteins (Myo1e and Myo1f), the latter displaying additional glycine-rich (TH2) and Src homology 3 (SH3) domains. These myosin motors can link membranes to the actin cytoskeleton via their tail domain. Beside the involvement of myosin 1 motors in a large variety of cellular processes, including cell migration and membrane trafficking (McIntosh and Ostap, 2016), manipulations of myosin 1 expression have revealed a correlation between myosin 1 proteins and the actin network architecture (Almeida et al., 2011; Capmany et al., 2019; Gupta et al., 2013; Iuliano et al., 2018; Joensuu et al., 2014). Recent experimental evidence from cell biological and *in vitro* biophysical approaches indicates that Myo1b can control the dynamics and architecture of the dendritic actin network (Almeida et al., 2011; Iuliano et al., 2018; Pernier et al., 2019, 2020). Given the various cytoplasmic regions where Myo1b has been localized, which include endosomes, the *trans*-Golgi network and plasma membrane (Almeida et al., 2011; Raposo et al., 1999; Salas-Cortes et al., 2005), we hypothesized that Myo1b interacts with partners that will regulate its motor activity in space and time.

In this report, we identified pleckstrin homology domain-containing family H member 1 with MyTH4 domain (Plekhh1, also known as MAX-1) as a partner of myosin 1 proteins and an effector of EphB2 receptors. Plekhh1 protein contains PH, MyTH4 and FERM domains and appears to localize to neuronal processes (Huang et al., 2002). It has been suggested that Plekhh1 contributes to netrin-induced axon repulsion by modulating the UNC-5 receptor signalling pathway in *Caenorhabditis elegans* (Huang et al., 2002) and acts upstream of the ephrin pathway in zebrafish (Zhong et al.,

[1]Institut Curie, PSL Research University and CNRS UMR144, 26 rue d'Ulm, 75005 Paris, France. [2]Sorbonne Université, 75005 Paris, France. [3]Laboratoire Physico-Chimie Curie, Institut Curie, PSL Research University, CNRS UMR168, 75005 Paris, France.

*Author for correspondence (evelyne.coudrier@curie.fr)

J.P., 0000-0002-0480-9355; H.L., 0000-0001-9090-7893; E.C., 0000-0001-6011-8922

Handling Editor: Michael Way
Received 17 April 2021; Accepted 26 October 2021

Journal of Cell Science (2021) 134, jcs258802. doi:10.1242/jcs.258802

2006). In this report we show that Plekhh1 interacts with two members of the myosin 1 family – Myo1b and Myo1c – and EphB2 receptors. Using cell culture, we analysed the role of Plekhh1 during cell repulsion induced by EphB2–ephrinB1 signalling. We compared the contribution of Plekhh1 to reorganization of the cortical actin network upon EphB2–ephrinB1 signalling with that of Myo1b and Myo1c, and we analysed its potential role in regulating Myo1b motor activity.

RESULTS

Plekhh1 is a partner of myosin 1 proteins and interacts with Myo1b via its N-terminal domain

Plekhh1 contains a N-terminal domain (Plekhh1-NTer) with a short coiled-coil domain that is highly homologous to that of Plekhh2 (Perisic et al., 2012), and a C-terminal domain (Plekhh1-CTer) with two PH motifs, a MyTH motif and a FERM domain (Fig. 1A). Using a yeast two-hybrid screen (data not shown), we identified a domain in the coiled-coil region of human Plekhh1 (amino acids 53–372; referred to here as the Plekkh1 interacting domain or Plekhh1-ID) (Fig. 1A) as a potential partner of Myo1b. This observation was first confirmed using pull-down experiments with GST-tagged Plekhh1-ID (Fig. 1B) and total Hek293T cell extracts expressing GFP–Myo1b, GFP–Myo1a or GFP–myosin 6 (GFP–Myo6). GST–Plekhh1-ID pulled down GFP–Myo1b and GFP–Myo1a, two related short-tail myosin 1 proteins, but not GFP–Myo6 (Fig. 1C, D). Using GFP-Trap, Myc–Plekhh1 was observed to co-immunoprecipitate with GFP–Myo1b and with another GFP-tagged short-tail myosin 1, GFP–myosin 1c (Myo1c), when the recombinant proteins were co-expressed in Hek293T cells (Fig. 1E,G). In contrast, Myc–Plekhh1 did not pull down the GFP tag alone (Fig. 1F).

We attempted to identify the domains of Plekhh1 that interact with Myo1b. A higher amount of Myc–Plekhh1-NTer than Myc–Plekhh1-CTer co-immunoprecipitated with GFP–Myo1b (Fig. 1H,I). We also analysed the ability of Myo1b domains to bind Plekhh1. Myo1b comprises a motor domain, an LCBD that binds calmodulin (IQ) and a tail domain at the C terminus (Fig. S1A). We quantified the amount of Myc–Plekhh1 that was pulled down with the different recombinant domains of GFP–Myo1b. A significantly higher amount of Myc–Plekhh1 co-immunoprecipitated with the GFP-tagged Myo1b tail domain (GFP–Myo1b-Tail) than with full-length GFP–Myo1b or the other GFP-tagged Myo1b domains (Fig. S1B,C).

Taken together, these pull-down experiments suggest that Plekhh1 is a partner of short-tail myosin 1 proteins and that Plekhh1 interacts with the tail domain of Myo1b via its N-terminal domain.

Plekhh1 is associated in part with the plasma membrane and focal adhesions

To analyse the role of Plekhh1, we generated polyclonal antibodies that specifically recognize endogenous Plekhh1. The anti-Plekhh1 antibodies detected a major band corresponding to a protein with a molecular mass of 159 kDa, which is consistent with the calculated molecular mass of Plekhh1 (151 kDa), in HCT116 cells expressing YFP–EphB2 (YFP–EphB2-HCT116) treated with control siRNA (Fig. S2A). This protein was not detected in cells treated with siRNA targeting Plekhh1 (Plekhh1 siRNA) (Fig. S2A), indicating that the polyclonal antibodies are specific for Plekhh1 in western blot experiments. Using these antibodies, we confirmed the interaction of GFP–Myo1b with endogenous Plekhh1 in Hek293T cells (Fig. S2B). We also analysed the tissue expression of Plekhh1 in mice. We observed that Plekhh1 is expressed in brain and intestine (Fig. S2C), but in contrast to Plekhh2, Plekhh1 was not detected in kidney (Fig. S2C) (Perisic et al., 2012).

Owing to a low signal to noise ratio, the polyclonal anti-Plekhh1 antibodies did not allow us to analyse the cellular distribution of Plekhh1 by immunofluorescence. We thus expressed GFP–Plekhh1 to study the cellular distribution of Plekhh1. When GFP–Plekhh1 was expressed in cells expressing endogenous Plekhh1, such as Hek293T or YFP–EphB2-HCT116 cells (Fig. 2A), it was mostly associated with aggregate-like structures concentrated in the perinuclear region of the cytoplasm (Fig. 2A). In contrast, when GFP–Plekhh1 was expressed in HeLa cells, where endogenous Plekhh1 was hardly detectable (Fig. 2A), we observed GFP–Plekhh1 at the plasma membrane in 63% of transfected cells (Fig. 2B) and its co-distribution with vinculin, a focal adhesion (FA) protein, in 37% of transfected cells (Fig. 2C), in addition to association with aggregate-like structures in the perinuclear region. By comparison, expression of the GFP tag alone resulted in diffuse localization in the cytoplasm and the nucleus (Fig. 2B).

Untagged Plekhh1 expressed in HeLa cells was also detected at the plasma membrane of the transfected cells and co-distributed with vinculin (Fig. S2D,E). However, untagged Plekhh1 expressed at a low level still formed aggregates in the perinuclear region (Fig. S2D,E). Given the 54% amino acid sequence identity shared by the coiled-coil domains of Plekhh1 (amino acids 28–168) and Plekhh2 (amino acids 27–167), the Plekhh1 aggregates may correspond to self-association via the coiled-coil domain, similar to that described previously for Plekhh2 (Perisic et al., 2012). Nevertheless, besides forming large aggregates in the cytoplasm and in the perinuclear region, Plekhh1 is also associated in part with the plasma membrane and FAs when it is expressed in cells where endogenous Plekhh1 is hardly detectable.

Plekhh1 contributes to cell repulsion

Using genetic approaches, Plekhh1 has previously been shown to contribute to cell repulsion induced by netrin–UNC-5 or EphB2–ephrinB signalling pathways (Huang et al., 2002; Zhong et al., 2006). We thus investigated whether Plekhh1 contributes to cell repulsion induced by EphB2–ephrinB1 signalling, for which we have previously shown the involvement of Myo1b (Prospéri et al., 2015). Using the experimental approaches described previously (Prospéri et al., 2015) with co-culture of HCT116 cells stably expressing mCherry–ephrinB1 or YFP–EphB2, we quantified the number of cell repulsions per cell–cell contact observed within 3 h depending on the expression of Plekhh1 in YFP–EphB2-HCT116 cells. We observed that the number of cell repulsion events decreased by 67% for EphB2-expressing cells treated with Plekhh1 siRNA compared to EphB2-expressing cells treated with control siRNA (Fig. 3; Movie 1).

Plekhh1 interaction with EphB2 is dependent on EphB2 kinase activity, and Plekhh1 is phosphorylated upon EphB2 stimulation

Since Plekhh1 contributes to cell repulsion induced by EphB2–ephrinB1 signalling, we then analysed whether Plekhh1 interacts with EphB2 in pull-down experiments. Flag-tagged EphB2 co-immunoprecipitated with GFP–Plekhh1 but not with GFP alone (Fig. 4A). We compared the ability of GFP–Plekhh1-NTer, GFP–Plekhh1-CTer (containing the PH, MyTH and FERM motifs), GFP–Plekhh1-MyTH-FERM and GFP–Plekhh1-FERM domains (Fig. 1A) to interact with Flag–EphB2. Although the levels of expression of GFP–Plekhh1-NTer and GFP–Plekhh1-CTer were similar (Fig. 4E, input), the amount of Flag–EphB2 pulled down by GFP–Plekhh1-CTer was more than 2-fold greater that that pulled down by GFP–Plekhh1-NTer (Fig. 4E,F). GFP–Plekhh1-MyTH-

Journal of Cell Science (2021) 134, jcs258802. doi:10.1242/jcs.258802

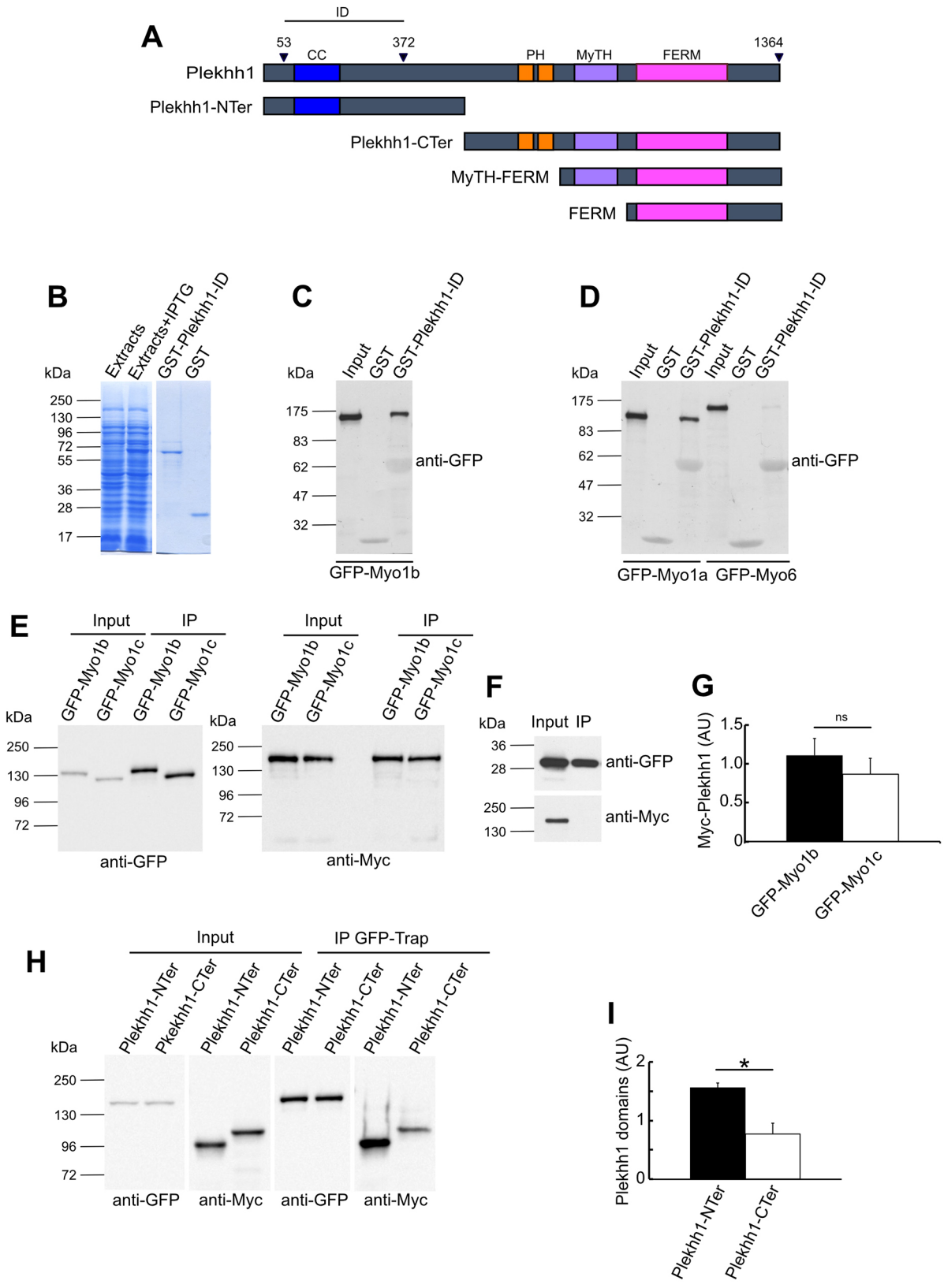

Fig. 1. See next page for legend.

FERM and GFP–Plekhh1-FERM pulled down similar amounts of Flag–EphB2 as GFP–Plekhh1-CTer (Fig. 4E,F), suggesting that the EphB2–Plekhh1 interaction occurs via the Plekhh1-CTer and in particular the FERM motif of this domain.

Next, we investigated whether the Plekhh1–EphB2 interaction requires EphB2 kinase activity. The amount of Flag-tagged kinase-deficient EphB2 mutant (Flag–EphB2-KD) pulled down by GFP–Plekhh1 was only 14.9% of the amount of Flag–EphB2

Journal of Cell Science (2021) 134, jcs258802. doi:10.1242/jcs.258802

Fig. 1. Plekhh1 is a partner of myosin 1 proteins and interacts with Myo1b via its N-terminal domain. (A) Schematic representation of Plekhh1 and Plekhh1 domains used in the experiments. CC, coiled-coil domain; ID, Pleckhh1-ID. (B) Coomassie Blue-stained SDS–PAGE gels showing *E. coli* extracts that were either untreated or treated with IPTG (left) and the purification of GST and GST–Plekhh1-ID from these *E. coli* extracts (right). (C) GFP–Myo1b pulled down with GST or GST–Plekhh1-ID from lysates of Hek293T cells expressing GFP–Myo1b (Input) was analysed using SDS–PAGE and immunoblotting with anti-GFP antibodies. (D) GFP–Myo1a and GFP–Myo6 pulled down with GST or GST–Plekhh1-ID from lysates of Hek293T cells expressing GFP–Myo1a or GFP–Myo6 (Input), respectively, were analysed using SDS–PAGE and immunoblotting with anti-GFP antibodies. (E) Myc–Plekhh1 co-immunoprecipitated (IP) from lysates of Hek293T cells expressing this recombinant protein and GFP–Myo1b or GFP–Myo1c (Input) was analysed using SDS–PAGE and immunoblotting with anti-GFP (left) and anti-Myc (right) antibodies. (F) Myc–Plekhh1 pulled down (IP) from lysates of Hek293T cells also expressing GFP (Input) was analysed using SDS–PAGE and immunoblotting with anti-GFP and anti-Myc antibodies. (G) The amount of Myc–Plekhh1 pulled down with GFP–Myo1b or GFP–Myo1c was quantified and normalized to the amount of GFP–Myo1b or GFP–Myo1c immunoprecipitated, respectively. Data are shown as the mean±s.e.m. of three experiments. ns, no significant difference between the two different experimental conditions (P=0.2122; two-tailed unpaired t-test with Welch's correction). (H) Myc–Plekhh1-NTer and Myc–Plekhh1-CTer pulled down with GFP–Myo1b (IP GFP-Trap) from lysates of Hek293T cells expressing these recombinant proteins (Input) were analysed using SDS–PAGE and immunoblotting with anti-GFP and anti-Myc antibodies. (I) The amount of Myc–Plekhh1-NTer or Myc–Plekhh1-CTer pulled down with GFP–Myo1b was quantified and normalized to the amount of GFP–Myo1b immunoprecipitated. Data are shown as the mean±s.e.m. of three experiments. *P=0.0328 (two-tailed unpaired t-test with Welch's correction). Input lanes represent 0.25% of the total lysate used for IP in C, 0.17% in D, and 0.5% in E–H. Data shown in B–D,F are representative of three experiments. AU, arbitrary units.

pulled down in control experiments (Fig. 4B,C), indicating that the Plekhh1–EphB2 interaction requires EphB2 kinase activity. Activated EphB2 can trigger Plekhh1 phosphorylation via its kinase activity or via another kinase activated by EphB2. Accordingly, the tyrosine phosphorylation of GFP–Plekhh1 decreased by 91% in cells expressing Flag–EphB2-KD compared to levels in Flag–EphB2-expressing cells (Fig. 4B,D). The amount of Flag–EphB2-KD pulled down by GFP–Plekhh1-NTer, GFP–Plekhh1-CTer and GFP–Plekhh1-MyTH-FERM was 34%, 41.2% and 40.7% lower, respectively, than the amount of Flag–EphB2 pulled down, whereas the amount of Flag–EphB2-KD pulled down by GFP–Plekhh1-FERM was 78% lower than the amount of Flag–EphB2 pulled down by the same construct (Fig. 4E,F), suggesting that the interaction between Plekhh1 and EphB2 that depends on EphB2 kinase activity occurs via the FERM domain of Plekhh1. Comparison of the tyrosine phosphorylation of the different GFP–Plekhh1 domains in the presence of Flag–EphB2 or Flag–EphB2-KD showed that only the tyrosine phosphorylation of Plekhh1–CTer was increased in the presence of wild-type EphB2, showing a 5-fold increase compared to levels in the presence of the kinase-deficient mutant (Fig. 4E,G). Taken together, these observations indicate that Plekhh1 interacts with EphB2 via its FERM domain, and that this interaction is dependent on EphB2 kinase activity. Furthermore, Plekhh1-CTer tyrosine phosphorylation increases, unlike that of Plekhh1-MyTH-FERM and Plekhh1-FERM, suggesting that when Plekhh1 interacts via its FERM domain with activated EphB2, it becomes phosphorylated on the proximal part of its C-terminal domain, including the PH motifs. This phosphorylation can occur directly, via the kinase activity of EphB2, or indirectly, via another kinase activated by EphB2.

We have previously reported that Hek293T cells do not present detectable endogenous EphB2 (Prospéri et al., 2015), although Myc–Plekhh1 was pulled down by GFP–Myo1b in these cells (Fig. 1A). This indicates that the Plekhh1–Myo1b interaction does not require EphB2 expression. Similarly, the interaction between EphB2 and Plekhh1 is independent of Myo1b expression; GFP–Plekhh1 co-immunoprecipitated with Flag–EphB2 in Hek293T cells treated with control siRNA or siRNA targeting Myo1b (Fig. S3). In summary, these pull-down experiments indicate that Myo1b interacts with Plekhh1-NTer, whereas EphB2 interacts with Plekhh1-CTer in a kinase activity-dependent manner.

Depletion of Plekhh1 decreases the formation of filopodia upon EphB2–ephrinB1 stimulation

We have previously reported that the cortical actin network is fully reorganized during cell repulsion, resulting in the formation of filopodia at contacts between cells expressing the receptor and cells expressing the ligand, and the formation of lamellipodia opposite the site of cell–cell contact (Prospéri et al., 2015). Taking advantage of clustered soluble recombinant ephrinB1–Fc, we investigated the role of Plekhh1 in the organization of the cortical actin network. As previously reported, cells treated with ephrinB1–Fc mimic the morphological changes that occur during cell repulsion induced by EphB2–ephrinB1 signalling (Prospéri et al., 2015); however, instead of inducing a directional signal that leads to the formation of filopodia at the contact between the ephrinB1- and EphB2-expressing cells and the formation of new lamellipodia opposite the site of contact, the ephrinB1–Fc signal is non-directional, with random modifications of the cortical actin network. In agreement with previous reports, cells treated with ephrinB1–Fc showed an important reorganization of the cortical actin network, with an increase in actin filaments below the plasma membrane and an increase in filopodia (Fig. 5A) (Prospéri et al., 2015; O'Neill et al., 2016). Depletion of Plekhh1 did not perturb the organization of actin filaments in non-stimulated cells. In contrast, depletion of Plekhh1 in cells stimulated with ephrinB1–Fc caused a decrease in filopodia and the formation of blebs (Fig. 5A). Analysis of stimulated cells treated with Plekhh1 siRNA and labelled with phalloidin, using confocal microscopy with a super-resolution module, confirmed the disorganization of the actin filaments underneath the plasma membrane compared to those in cells treated with control siRNA (Fig. 5B; Movies 2,3). We quantified the number of filopodia per cell to assess the effects of ephrinB1–Fc treatment and the expression levels of Plekhh1. The number of filopodia was similar in cells treated with control siRNA or Plekhh1 siRNA in non-stimulated conditions. In contrast, depletion of Plekhh1 in stimulated cells decreased the number of filopodia per cell to nearly reach the number of filopodia observed in the absence of ephrinB1–Fc (Fig. 6A). The number of filopodia formed in these experimental conditions was rescued by the expression of a recombinant mCherry-tagged Plekhh1 that was insensitive to the siRNA (Fig. 6B). In contrast, the number of filopodia was not rescued by the expression of Plekhh1-CTer, which interacts with EphB2 and is phosphorylated depending on EphB2 kinase activity (Fig. 6B). Thus Plekhh1, like Myo1b (Prospéri et al., 2015), contributes to the formation of filopodia upon EphB2 stimulation. Moreover, our observations suggest that Plekhh1-NTer, which binds to Myo1b, is required for the formation of filopodia upon EphB2 stimulation.

Depletion of Plekhh1 and myosin 1 proteins increases the number of blebs formed upon EphB2–ephrinB1 stimulation

Analysis of stimulated cells treated with Plekhh1 siRNA revealed an increase in bleb formation compared to that of cells treated with

Journal of Cell Science (2021) 134, jcs258802. doi:10.1242/jcs.258802

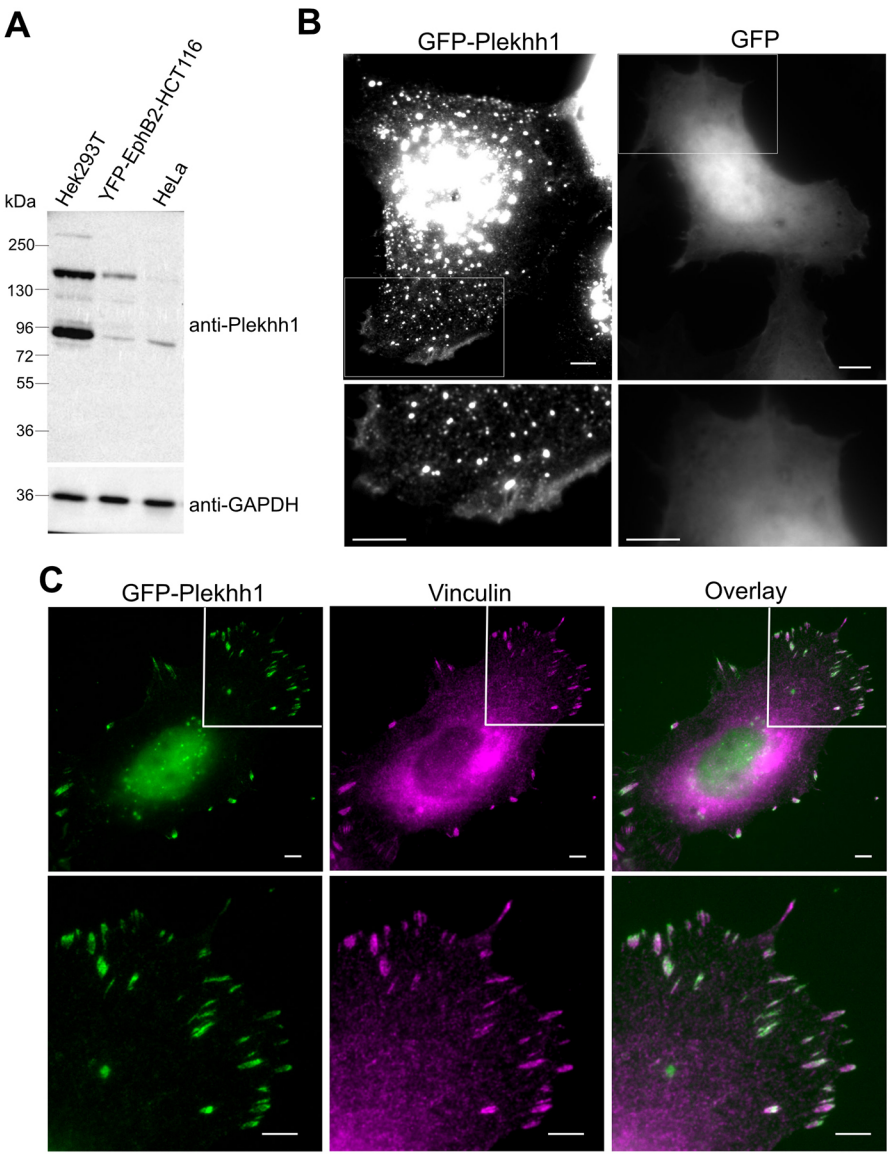

Fig. 2. GFP–Plekhh1 is associated with plasma membrane and FAs. (A) Detection of Plekhh1 in Hek293T, YFP–EphB2-HCT116 and HeLa cell lysates after SDS–PAGE and immunoblotting using specific anti-Plekhh1 antibodies and an anti-GAPDH antibody for a loading control. Blots shown are representative of three experiments. (B) Cellular distribution of GFP–Plekhh1 or GFP expressed in HeLa cells, analysed by epifluorescence microscopy. White boxes mark regions shown in the row below enlarged by a scale factor of 1.7. (C) Comparison of the distribution of GFP–Plekhh1 and vinculin in HeLa cells, analysed by epifluorescence microscopy. White boxes mark regions shown in the row below enlarged by a scale factor of 2.1. Note that GFP–Plekhh1 co-distributes in part with vinculin (white in overlay images). Images in B and C are representative of three experiments. Scale bars: 5 µm.

control siRNA (Fig. 5; Movies 2,3). We quantified the percentage of cells exhibiting blebs to assess the effects of ephrinB1–Fc treatment and Plekhh1 depletion. Depletion of Plekhh1 did not change the percentage of non-stimulated cells with blebs (Fig. 6C). The increase in the percentage of cells with blebs upon stimulation for cells treated with control siRNA was also non-significant (P=0.0817; Fig. 6C). However, in the presence of ephrinB1–Fc, the percentage of Plekhh1 siRNA-treated cells with blebs was 3.8-fold greater than the percentage of control siRNA-treated cells with blebs (Fig. 6C). Expression of recombinant mCherry–Plekhh1 insensitive to the siRNA in stimulated cells treated with Plekhh1 siRNA partly rescued the limited formation of blebs observed in cells treated with control siRNA, whereas expression of Plekhh1-CTer, which interacts with EphB2 but not Myo1b, did not rescue the limited number of blebs (Fig. 6D). Thus, the interaction of Plekhh1 with Myo1b could be important to restrict the formation of blebs upon EphB2 stimulation.

Bleb formation can rely on a local decrease in membrane–cortex attachments. Owing to their ability to bind membrane, myosin 1 proteins contribute to membrane–cortex attachments, and thus, these motors may directly control the formation of blebs. We therefore analysed whether knockdown of Myo1b or Myo1c after EphB2 stimulation resulted in the formation of blebs. Non-stimulated cells treated with control, Myo1b or Myo1c siRNAs presented no significant differences in the percentage of cells with blebs (Fig. 6E,G). The increase in the percentage of control siRNA-treated cells with blebs upon EphB2 stimulation compared to non-stimulated cells was also non-significant (P=0.1752 and P=1 for Myo1b and Myo1c experiments, respectively) (Fig. 6E and G). However, the percentage of stimulated cells with blebs increased by 3- and 2.8-fold for cells treated with Myo1b or Myo1c siRNAs, respectively, compared to stimulated cells treated with control siRNA (Fig. 6E–H). Thus, both Myo1b and Myo1c are required to restrict the formation of blebs upon the reorganization of the cortical actin network after EphB2 stimulation. Interestingly, more than 60% of stimulated cells exhibited blebs in the absence of Plekhh1, whereas only 30% were observed to have blebs in the absence of Myo1b or Myo1c, suggesting that expression of both Myo1b and Myo1c reduces the formation of blebs during EphB2 stimulation.

Journal of Cell Science (2021) 134, jcs258802. doi:10.1242/jcs.258802

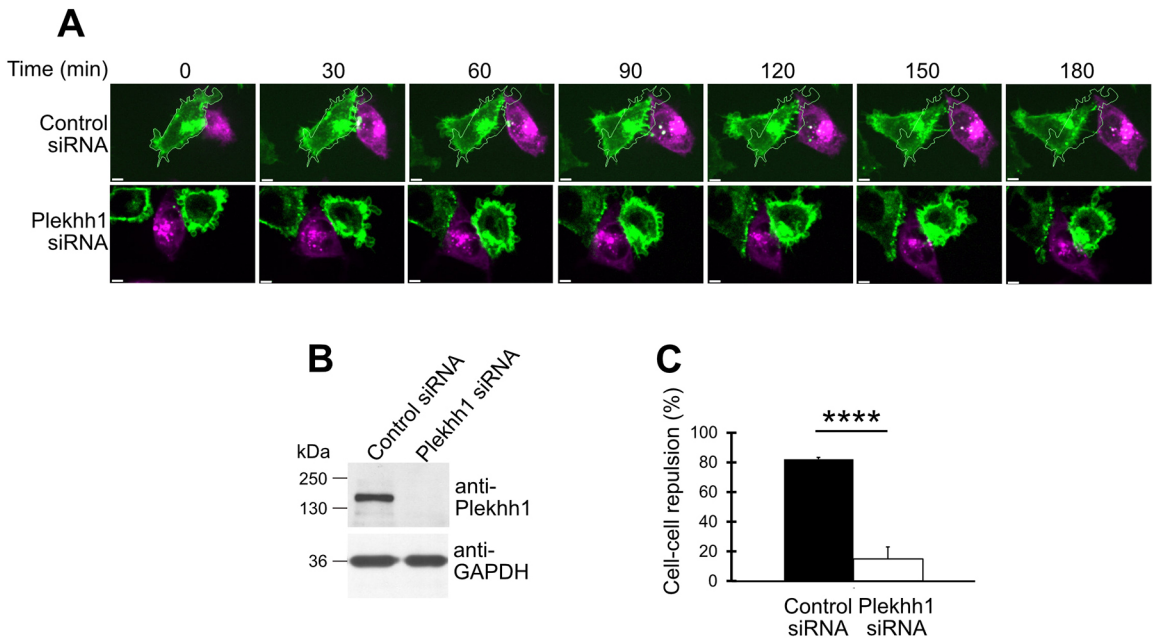

Fig. 3. Plekhh1 regulates cell repulsion induced by EphB2–ephrinB1 signalling. (A) Time-lapse images of YFP–EphB2-HCT116 cells (green) treated with control or Plekhh1 siRNAs co-cultured with mCherry–ephrinB1-HCT116 cells (magenta) (see also Movie 1). The white lines in the top panel correspond to the outline of the first position of the YFP–EphB2-HCT116 cell. Scale bars: 5 µm. (B) Detection of endogenous Plekhh1 in YFP–EphB2-HCT116 cells treated with control or Plekhh1 siRNAs for 48 h, as used for the analyses in A and C. Cell lysates were analysed using SDS–PAGE and immunoblotting with specific anti-Plekhh1 antibodies. An anti-GAPDH antibody was used as a loading control. Blots shown are representative of three experiments. (C) Cell repulsion events as a percentage of cell–cell contacts observed during 3 h time-lapse imaging (as described in A) in the presence or absence of Plekhh1 (n=28 and n=32, respectively). Data are shown as the mean±s.e.m. of three experiments. ****P= 3.077×10^{-7} (Fisher's exact test).

Plekhh1 and myosin 1 proteins control the length of FAs after stimulation of EphB2 receptors

Like filopodia, FAs also rely on the organization and dynamics of the cortical actin network (Sackmann, 2015; Schaks et al., 2019). Because Plekhh1 is associated in part with FAs (Fig. 2C), we next investigated the impact of Plekhh1 on FAs upon EphB2 stimulation. We determined for each cell in the different experimental conditions the average value of the length of FAs – YFP–EphB2-HCT116 cells with or without knockdown of Plekhh1, Myo1b or Myo1c that were stimulated or not with ephrinB1–Fc (Fig. 7). To determine whether variation in the average length of FAs in the different experimental conditions was due to variation of a subpopulation of FAs or not, we also analysed the distribution of the length of the FAs using empirical cumulative density functions (ECDFs; see Materials and Methods) (Fig. S4). EphB2 stimulation increased the average length of FAs, spread their length distribution and shifted them towards longer lengths in YFP–EphB2-HCT116 cells (Fig. 7A,B; Fig. S4A). Depletion of Plekhh1, Myo1b or Myo1c in stimulated cells reduced the average length of FAs and shifted their distribution towards shorter FA lengths (Fig. 7C,D,G,H; Fig. S4B,C,E,F). The impact of depletion of Plekhh1 on the length (average length and distribution) of FAs was rescued to some extent by expression of a recombinant Plekhh1 that was insensitive to the Plekhh1 siRNA (Fig. 7E; Fig. S4D). Surprisingly, Plekhh1-CTer rescued the average length of FAs better than full-length Plekhh1 (Fig. 7E; Fig. S4D), although we could not detect this recombinant domain in the FAs, in contrast to Plekhh1-NTer (Fig. S5). However, we noticed that expression of the Plekhh1-CTer domain alone in YFP–EphB2-HCT116 cells elongated FAs even in the absence of stimulation, indicating that the expression of this domain has a side effect on the length of FAs (Fig. 7F). Taken together, these observations indicate that Plekhh1 and myosin 1 proteins control the length of FAs in EphB2-stimulated cells.

The Plekhh1 interacting domain increases motor activity of Myo1b *in vitro*

We have previously reported that Myo1b acts as an actin depolymerase and debranches the Arp2/3-mediated branched actin network due to its motor activity (Pernier et al., 2019, 2020). We thus wondered whether Myo1b interaction with Plekhh1 can affect its motor activity. We could not produce a recombinant full-length Plekhh1, but given the fact that GST–Plekhh1-ID pulled down GFP–Myo1b (Fig. 1B), we investigated the impact of this domain on the motor activity of Myo1b. We used TIRF microscopy to analyse the velocity of sliding actin filaments stabilized with phalloidin (F-actin) on Myo1b bound to a glass substrate at a density of 8000/µm^2 in the presence of GST or GST–Plekhh1-ID (Pernier et al., 2019). As previously reported (Pernier et al., 2019, 2020), the sliding velocity of F-actin on Myo1b was on average 55 nm/s (Fig. 8). Addition of GST increased the sliding velocity of F-actin; however, increasing the amount of GST did not significantly change the velocity of the actin filaments (Fig. 8). Thus, the impact of GST was dose independent, and its interaction with the actin filament can be considered random (Fig. 8). In contrast, addition of GST–Plekhh1-ID significantly increased the velocity of stabilized F-actin by 73% compared to the addition of GST, and the increase was observed to be dose dependent (Fig. 8). In agreement with previous reports showing that manipulation of the tail domain of myosin 1 proteins modifies their motor activity (Laakso et al., 2010), the binding of Plekhh1 with the tail of Myo1b can control the motor activity of Myo1b and thereby regulate actin dynamics.

DISCUSSION

In this work, we show that Plekhh1 is an effector of EphB2. Plekhh1 interaction with EphB2 is dependent on EphB2 kinase activity, and Plekhh1 is phosphorylated upon EphB2 stimulation. Plekhh1 also

Journal of Cell Science (2021) 134, jcs258802. doi:10.1242/jcs.258802

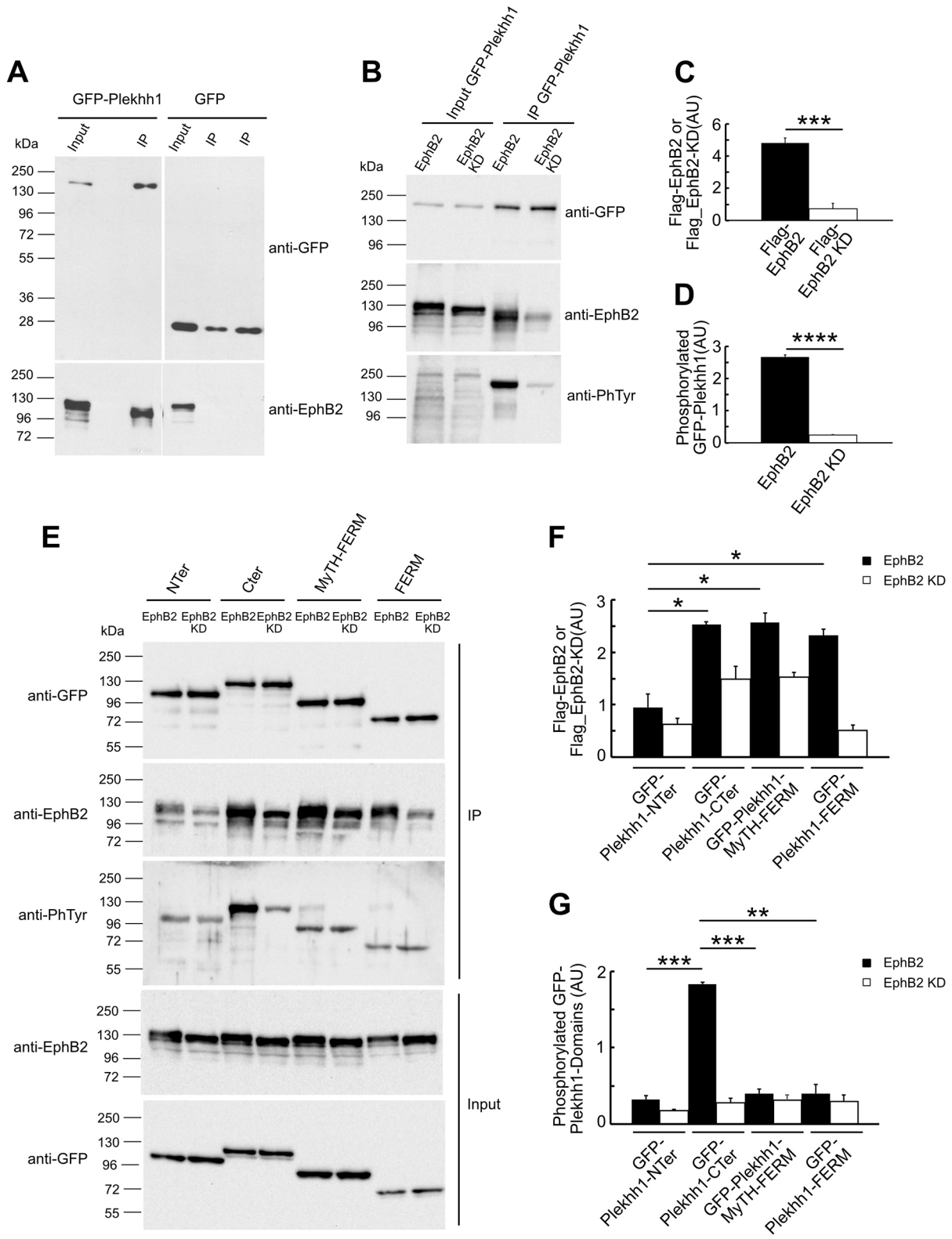

Fig. 4. See next page for legend.

contributes to cell repulsion and controls the organization of cortical actin in response to EphB2–ephrinB1 signalling. Stimulation of EphB2 receptors induces the formation of filopodia and the elongation of FAs. We show that absence of Plekhh1 decreases the formation of filopodia and reduces the average length of FAs. In addition, absence of Plekhh1 increases the formation of blebs in these experimental conditions.

Plekhh1 is localized in part at the plasma membrane and FAs. Interestingly, Plekhh2 also localizes to FAs (Perisic et al., 2012). However, Plekhh2 interaction with FAs depends on the FERM

Journal of Cell Science (2021) 134, jcs258802. doi:10.1242/jcs.258802

Fig. 4. Plekhh1-CTer interacts with EphB2, and this requires EphB2 kinase activity. (A) Flag–EphB2 pulled down (IP) with GFP–Plekhh1 or GFP from lysates of Hek293T cells expressing these recombinant proteins (Input) was analysed using SDS–PAGE and immunoblotting with anti-GFP and anti-EphB2 antibodies. Data shown are representative of three experiments. (B) Flag–EphB2 (EphB2) or Flag–EphB2-KD (EphB2 KD) pulled down (IP) with GFP–Plekhh1 from lysates of Hek293T cells expressing these recombinant proteins (Input) were analysed using SDS–PAGE and immunoblotting with anti-GFP, anti-EphB2 and anti-phosphotyrosine (anti-PhTyr) antibodies. (C) The amount of Flag–EphB2 and Flag–EphB2-KD pulled down with GFP–Plekhh1 was quantified and normalized to the amount of GFP–Plekhh1 immunoprecipitated. Data are shown as the mean±s.e.m. of three experiments. ***P=0.009. (D) The amount of tyrosine-phosphorylated GFP–Plekhh1 pulled down with Flag–EphB2 or Flag–EphB2 kinase-deficient mutant was quantified and normalized to the amount of GFP–Plekhh1 immunoprecipitated. Data are shown as the mean±s.e.m. of three experiments. ****P<0.0001. (E) Flag–EphB2 or Flag–EphB2-KD pulled down (IP) from lysates of Hek293T cells expressing these recombinant proteins and GFP–Plekhh1-NTer, GFP–Plekhh1-CTer, GFP–Plekhh1-MyTH-FERM or GFP–Plekhh1-FERM (Input) were analysed using SDS–PAGE and immunoblotting with anti-GFP, anti-EphB2 and anti-phosphotyrosine antibodies. (F) The amounts of Flag–EphB2 and Flag–EphB2-KD pulled down with GFP–Plekhh1-NTer, GFP–Plekhh1-CTer, GFP–Plekhh1-MyTH-FERM or GFP–Plekhh1-FERM were quantified and normalized to the amounts of the different GFP–Plekhh1 domains immunoprecipitated. Data are shown as the mean±s.e.m. of three experiments. *P=0.0227 for GFP–Plekhh1-NTer and GFP–Plekhh1-CTer; *P=0.0110 for GFP–Plekhh1-NTer and GFP–Plekhh1-MyTH-FERM; *P=0.0222 for GFP–Plekhh1-NTer and GFP–Plekhh1-FERM. (G) The amount of tyrosine phosphorylated GFP–Plekhh1-NTer, GFP–Plekhh1-CTer, GFP–Plekhh1-MyTH-FERM or GFP–Plekhh1-FERM pulled down with Flag–EphB2 or Flag–EphB2-KD was quantified and normalized to the amount of the different GFP–Plekhh1 domains immunoprecipitated. Data are shown as the mean±s.e.m. of three experiments ***P=0.0001 for GFP–Plekhh1-NTer and GFP–Plekhh1-CTer; ***P=0.0001 for GFP–Plekhh1-CTer and GFP–Plekhh1-MyTH-FERM; **P=0.0022 for GFP–Plekhh1-CTer and GFP–Plekhh1-FERM. Input lanes in A, B and E represent 0.5% of the total lysate. A two-tailed unpaired *t*-test with Welch's correction was used for statistical testing. AU, arbitrary units.

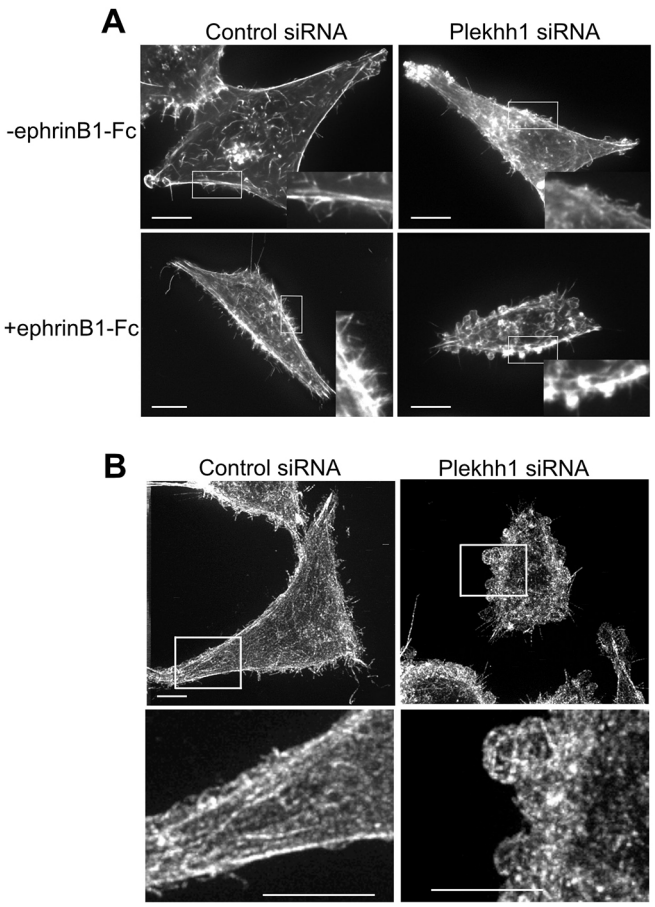

Fig. 5. Depletion of Plekhh1 in cells stimulated by ephrinB1–Fc perturbs the cortical actin network. (A) Distribution of F-actin filaments visualized using fluorescently labelled phalloidin in YFP–EphB2-HCT116 cells treated with control or Plekhh1 siRNAs in the presence or absence of ephrin B1–Fc. Cells were analysed using 3D deconvolution microscopy. Images represent *Z* projections of 41 images. White boxes mark regions shown in the inserts enlarged by scale factors of 1.5 and 2.5 for the horizontal and vertical boxes, respectively. Scale bars: 10 µm. (B) Distribution of F-actin filaments visualized using fluorescently labelled phalloidin in YFP–EphB2-HCT116 cells treated with control or Plekhh1 siRNAs in the presence of ephrin B1–Fc. Cells were analysed using confocal microscopy with a super-resolution module. Images represent the first plane of 3D reconstruction (see also Movies 2 and 3). White boxes in the top row of images mark regions shown in the row below enlarged by a scale factor of 3.7. Scale bars: 5 µm. Images in A and B are representative of two experiments.

domain in its C-terminal domain, whereas Plekhh1-Nter, but not Plekhh1-CTer, is in part associated with FAs (Fig. S5). Plekhh1-CTer binds EphB2 and is phosphorylated depending on EphB2 kinase activity, but this Plekhh1 domain does not rescue the formation of filopodia and does not reduce the formation of blebs in the absence of Plekhh1. Furthermore, Plekhh1-CTer has a side effect on the length of FAs independently of the expression of Plekhh1. Thus, these observations indicate that the role of Plekhh1 in the formation of filopodia, the elongation of FAs and the limitation of the formation of blebs upon EphB2 stimulation relies on Plekhh1-NTer.

Our data also demonstrate that Plekhh1 is a partner of myosin 1 proteins and that this interaction depends on Plekhh1-NTer. It is unlikely that the association of Plekhh1 with the perinuclear region is due to its interaction with nuclear myosin 1 (Percipalle and Farrants, 2006) because Plekhh1-NTer, which interacts with Myo1b, is not detected in the nucleus (Fig. S5). Myosin 1 proteins can both interact with the plasma membrane and control the architecture of actin networks (Almeida et al., 2011; Capmany et al., 2019; Gupta et al., 2013; Iuliano et al., 2018; Joensuu et al., 2014). We have previously reported that Myo1b contributes to the formation of filopodia (Prospéri et al., 2015), and we report in this work that both Myo1b and Myo1c contribute to the elongation of FAs upon stimulation of EphB2 receptors. Moreover, depletion of Myo1b or Myo1c contributes to the formation of blebs upon the stimulation of EphB2 receptors. We cannot exclude that Plekhh1 acts directly on the dynamics of the cortical actin network after its phosphorylation upon EphB2 stimulation, leading to the formation of filopodia, the elongation of FAs and the limitation of blebs. However, our data strongly suggest that the role of Plekhh1 on filopodia, blebs and FAs relies on its interaction with myosin 1 proteins via its N-terminal domain. In addition to previously demonstrating that Myo1b controls the formation of filopodia, we have also shown that *in vitro*, Myo1b mediates Arp2/3-dependent actin network debranching (Pernier et al., 2020; Prospéri et al., 2015). In this work, we report that Plekhh1-ID increases the motor activity of Myo1b *in vitro*. Thus, Plekhh1 interacting with Myo1b may activate the motor activity of Myo1b and consequently favour the debranching of Arp2/3-dependent actin networks to form filopodia. It has been previously reported that EphB2 stimulation induces a ROCK-dependent increase of the cortical actin network and induces the formation of actomyosin fibres (O'Neill et al., 2016). Moreover, the motor activity of Myo1b controls the formation of actomyosin fibres after EphB2 stimulation

Journal of Cell Science (2021) 134, jcs258802. doi:10.1242/jcs.258802

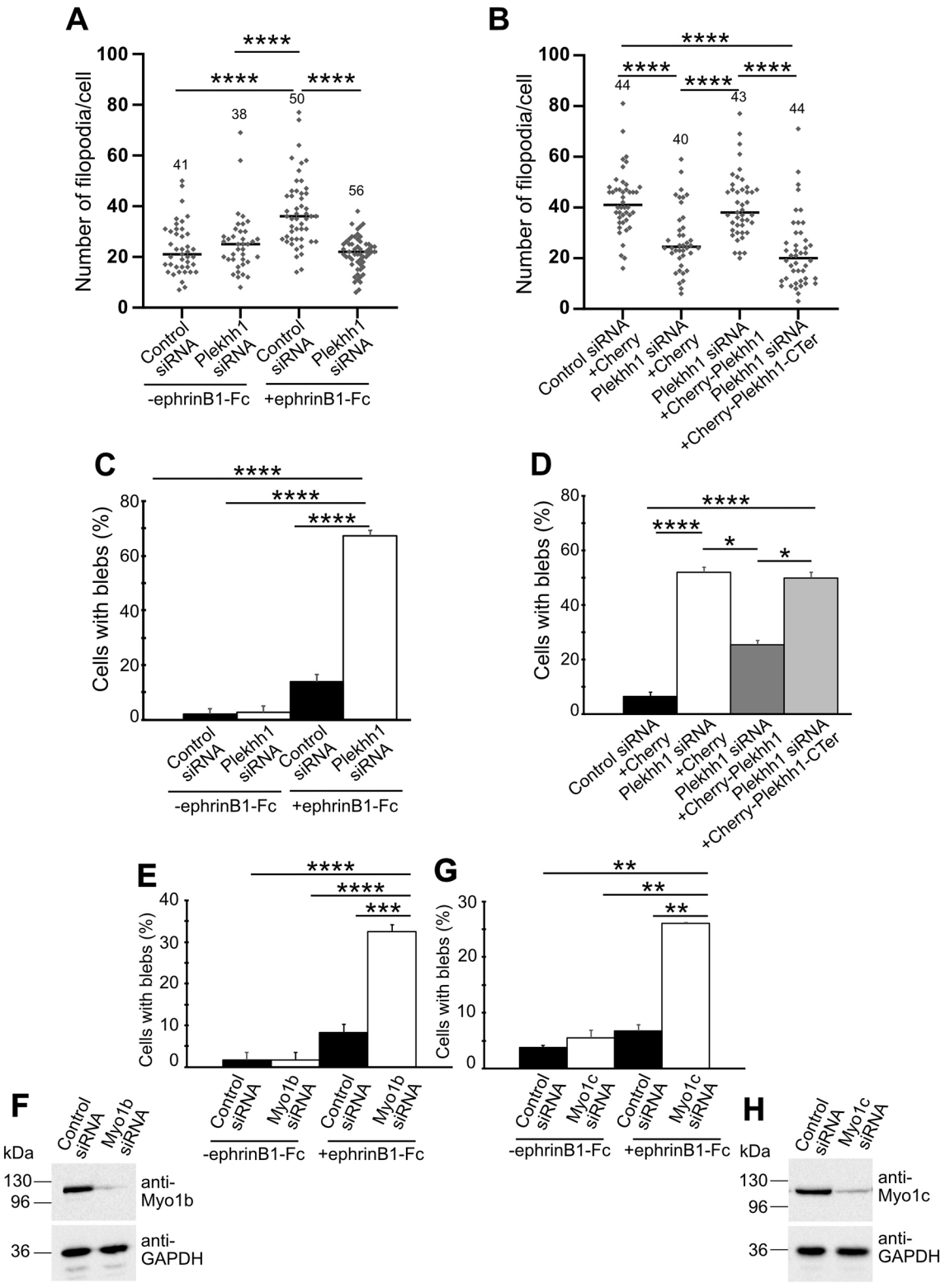

Fig. 6. See next page for legend.

(Prospéri et al., 2015). By interacting with Myo1b and controlling its motor activity, Plekhh1 can regulate the formation of actomyosin fibres and thereby regulate the formation of blebs. Recent experimental evidence supports that EphB2–ephrinB signalling results in an increase in cortical tension related to non-muscle myosin II (Kindberg et al., 2021). The length of FAs is also highly regulated by the force exerted by the actomyosin fibres (Aguilar-Cuenca et al., 2014). By controlling Myo1b motor activity, Plekhh1 can regulate the formation of actomyosin fibres and, consequently, the elongation of FAs.

In conclusion, using a cellular model that allows the study of non-directional EphB2 signalling, we identified a new partner of myosin

Journal of Cell Science (2021) 134, jcs258802. doi:10.1242/jcs.258802

Fig. 6. Depletion of Plekhh1 and myosin 1 proteins decreases filopodia and increases blebs in cells stimulated by ephrinB1–Fc. (A) Scatter plot of the number of filopodia per cell for YFP–EphB2-HCT116 cells stimulated or not with ephrinB1–Fc and treated with control or Plekhh1 siRNAs, as indicated. Data shown are the results of two experiments, and the median is indicated (non-stimulated control siRNA, *n*=41; non-stimulated Plekhh1 siRNA, *n*=38; stimulated control siRNA, *n*=50; stimulated Plekhh1 siRNA, *n*=56). ****$P<0.0001$. (B) Scatter plot of the number of filopodia per cell for YFP–EphB2-HCT116 cells stimulated with ephrinB1–Fc and co-transfected with control or Plekhh1 siRNAs and plasmids encoding mCherry, or siRNA-insensitive forms of mCherry–Plekhh1 and mCherry–Plekhh1-CTer, as indicated. Data shown are the results of two experiments, and the median is indicated (control siRNA and mCherry, *n*=44; Plekhh1 siRNA and mCherry, *n*=40; Plekkh1 siRNA and mCherry–Plekhh1, *n*=43; Plekhh1 siRNA and mCherry–Plekhh1-CTer, *n*=44). ****$P<0.0001$. (C) Percentage of cells showing blebs for YFP–EphB2-HCT116 cells stimulated or not with ephrinB1–Fc and treated with control or Plekhh1 siRNAs. Data are presented as the mean±s.e.m. percentage of cells with blebs from two experiments (non-stimulated control siRNA, *n*=41; non-stimulated Plekhh1 siRNA, *n*=38; stimulated control siRNA, *n*=48; stimulated Plekhh1 siRNA, *n*=56). ****$P=2.304\times10^{-11}$ for control siRNA −ephrinB1–Fc and Plekhh1 siRNA +ephrinB1–FC, ****$P=2.304\times10^{-11}$ for Plekhh1 siRNA −ephrinB1–FC and Plekhh1 siRNA +ephrinB1–FC, ****$P=7.842\times10^{-8}$ for control siRNA +ephrinB1–FC and Plekhh1 siRNA +ephrinB1–FC. (D) Percentage of cells showing blebs for YFP–EphB2-HCT116 cells stimulated with ephrinB1–Fc and co-transfected with control or Plekhh1 siRNAs and plasmids encoding mCherry, or siRNA-insensitive mCherry–Plekhh1 and mCherry–Plekhh1-CTer, as indicated. Data are presented as the mean±s.e.m. percentage of cells with blebs from two experiments (control siRNA and mCherry, *n*=45; Plekhh1 siRNA and mCherry, *n*=50; Plekkh1 siRNA and mCherry–Plekhh1, *n*=43; Plekhh1 siRNA and mCherry–Plekhh1-CTer, *n*=44). ****$P=1.287\times10^{-5}$ for control siRNA+mCherry and Plekhh1 siRNA+mCherry, ****$P=1.287\times10^{-5}$ for control siRNA+mCherry and Plekhh1 siRNA+mCherry–Plekhh1-CTer, *$P=0.02835$ for Plekhh1 siRNA+mCherry and Plekhh1 siRNA+mCherry–Plekhh1, *$P=0.03234$ for Plekhh1 siRNA+mCherry–Plekhh1 and Plekhh1 siRNA+mCherry–Plekhh1-CTer. (E) Percentage of cells with blebs for YFP–EphB2-HCT116 cells stimulated or not with ephrinB1–Fc and treated with control or Myo1b siRNAs. Data are presented as the mean±s.e.m. percentage of cells with blebs from two experiments (non-stimulated control siRNA, *n*=53; non-stimulated Myo1b siRNA, *n*=55; stimulated control siRNA, *n*=81; stimulated Myo1b siRNA, *n*=86). ****$P=9.558\times10^{-6}$ for control siRNA −ephrinB1–Fc and Myo1b siRNA +ephrinB1–Fc, ****$P=9.558\times10^{-6}$ for Myo1b siRNA −ephrinB1–Fc and Myo1b siRNA +ephrinB1-Fc, and ***$P=0.0002635$ for control siRNA −ephrinB1–Fc and Myo1b siRNA +ephrinB1–Fc. (F) YFP–EphB2-HCT116 cells treated with control or Myo1b siRNAs were analysed by SDS–PAGE and immunoblotting with anti-Myo1b antibodies or anti-GAPDH antibody as a loading control. (G) Percentage of cells with blebs for YFP–EphB2-HCT116 cells stimulated or not with ephrinB1–Fc and treated with control or Myo1c siRNAs. Data are presented as the mean±s.e.m. percentage of cells with blebs from two experiments (non-stimulated control siRNA, *n*=53; non-stimulated Myo1c siRNA, *n*=53; stimulated control siRNA, *n*=74; stimulated Myo1c siRNA, *n*=73). **$P=0.003951$ for control siRNA −ephrinB1–Fc and Myo1c siRNA +ephrinB1–Fc, **$P=0.007293$ for Myo1c siRNA −ephrinB1–Fc and Myo1c siRNA +ephrinB1–Fc, **$P=0.005081$ for control siRNA +ephrinB1–Fc and Myo1c siRNA +ephrinB1–Fc. (H) YFP–EphB2-HCT116 cells treated with control or Myo1c siRNAs were analysed by SDS–PAGE and immunoblotting with anti-Myo1c antibodies or anti-GAPDH antibody as a loading control. A non-parametric Kruskal–Wallis test followed by Dunn's multiple comparison test (A,B) and a Fisher's exact test with Benjamini–Hochberg multiple comparison correction (C–E,G) were used for statistical testing.

1 proteins that regulates their motor activity. This work gives new insight into the role of Plekhh1 and myosin 1 proteins in cell repulsion and the reorganization of cortical actin networks upon EphB2–ephrinB1 signalling. As a partner of myosin 1 proteins, Plekhh1 may activate myosin 1 motor activity when activated by tyrosine phosphorylation. Consequently, Plekhh1 can control the dynamic reorganization of the actin network induced by the motor activity of myosin 1 proteins in specific membrane domains of the cytoplasm. Studying the role of Plekhh1 in tissues or a cellular model of directional EphB2 signalling will be a future challenge.

MATERIALS AND METHODS

Antibodies and reagents

The following antibodies were used: homemade anti-Myo1b polyclonal antibody (1:1000 for western blot; Almeida et al., 2011), anti-Myo1c mouse monoclonal (1:200 for western blot; sc-136544; Santa Cruz Biotechnologies, Dallas, TX, USA), anti-phosphotyrosine mouse monoclonal (mAb; 1:1000 for western blot; clone 4G10; antibody platform of the Institut Curie, Paris, France), anti-GFP mouse monoclonal (mAb; 1:1000 for western blot; catalogue number 11814460001; Roche, Bâle, Switzerland); anti-Myc mouse monoclonal (mAb; 1:1000 for western blot; clone 9E10, antibody platform of the Institut Curie), anti-GADPH polyclonal rabbit antibody (pAb; 1:20,000 for western blot; catalogue number G9545; Sigma-Aldrich, St Louis, MO, USA), anti-vinculin mouse monoclonal (1:1000 for immunofluorescence; V9131; Sigma-Aldrich), anti-EphB2 polyclonal antibody (0.5 µg/ml; catalogue number AF467; R&D Systems, Minneapolis, MN, USA). The homemade anti-Plekhh1 polyclonal rabbit antibody was generated against the peptide C^{548}SLDSDYSEPEHKLQR^{563} and affinity purified with the recombinant protein GST–Plekhh1(53–597) (pAb; 1:1000 for western blot). We also used Alexa Fluor 546- or Alexa Fluor 647-coupled secondary antibodies against mouse IgG (1:400; catalogue number 715-165-151, Jackson ImmunoResearch) and horseradish peroxidase-conjugated secondary antibodies against mouse, rabbit or goat IgGs (1:5000; Invitrogen, Eugene, OR, USA). Alexa Fluor 546- or Alexa Fluor 647-conjugated phalloidin was used to detect F-actin (1:400; Invitrogen).

cDNA constructs

GST–Plekhh1-ID (amino acids 157–1119) was generated by cloning, at FseI and AscI sites of a modified pGEX-CS2 (gift from Alexis Gautreau, Ecole polytechnique, Palaiseau, France), a DNA fragment generated by PCR of human Plekhh1 (NCBI accession number NM_020715) using 5′ primer 5′-GCAGAGCAGAGAGCAGAGAAC-3′ and 3′ primer 5′-TTATTCCTCCCGGGACCTAGCTCG-3′. GST–Plekhh1(157–1791) for antibody purification was generated by cloning, at the same sites in the same vector, a DNA fragment generated by PCR on human Plekhh1 with 5′ primer 5′-GCAGAGCAGAGAGCAGAGAAC-3′ and 3′ primer 5′-TTACCTCTTCCACGTCTTCACCTG-3′. pCS2-Myc–Plekhh1 and pCS2-Plekhh1 were generated by cloning, at FseI and AscI sites of pCS2 and a modified pMyc-CS2 (gift from Alexis Gautreau), a DNA fragment generated by PCR on human Plekhh1 with 5′ primer 5′-ATGGCAGAACT-CAAGGTGGAGGCG-3′ and 3′ primer 5′-TCACAGCAACGTTGGC-CCCTTGGT-3′. pCS2-Myc–Plekhh1-NTer (amino acids 1–1617) and pCS2-Myc–Plekhh1-CTer (amino acids 1618–4095) were generated with NEBuilder HiFi DNA Assembly Cloning Kit (New England Biolabs, Ipswich, MA, USA) by cloning at FseI and AscI sites of pMyc-CS2 a DNA fragment generated by PCR on human Plekhh1 with 5′ primers 5′-aggacttgaattcaggccggcccATGGCAGAACTCAAGGTGG-3′ and 5′-aggacttgaattcaggccggcccGACTACGCCATCCCCCCG-3′, respectively, and 3′ primers 5′-actcactatagttctagaggcgcgccTCAACCCTCGGAGCTC-AG-3′ and 5′-actcactatagttctagaggcgcgccTCACAGCAACGTTGGC-CC-3′, respectively (where lowercase letters represent the sequence of the vector and uppercase letters represent the sequence of the gene). pmCherry-C1 Plekhh1 was generated with the same kit by cloning at EcoRI and SalI sites of pmCherry-C1 (Clontech, Mountain View, CA, USA) a DNA fragment generated by PCR of human Plekhh1 with 5′ primer 5′-gatctcgagctcaagcttcgaattctATGGCAGAACTCAAGGTGGAG-3′ and 3′ primer 5′-atcccgggcccgcggtaccgtcgacTCACAGCAACGTTGGCCC-3′. Five silent mutations were introduced in the sequence targeted by the Plekhh1 siRNA (C^{1542}AGGAAGACCAGCGGACTA^{1560}) by site-directed mutagenesis (New England Biolabs, Q5 Site-Directed Mutagenesis Kit) to give CAG**A**AA**A**AC**A**AG**T**GG**T**CTA (where bold characters indicate the mutated bases) in order to produce constructs insensitive to the siRNA.

Journal of Cell Science (2021) 134, jcs258802. doi:10.1242/jcs.258802

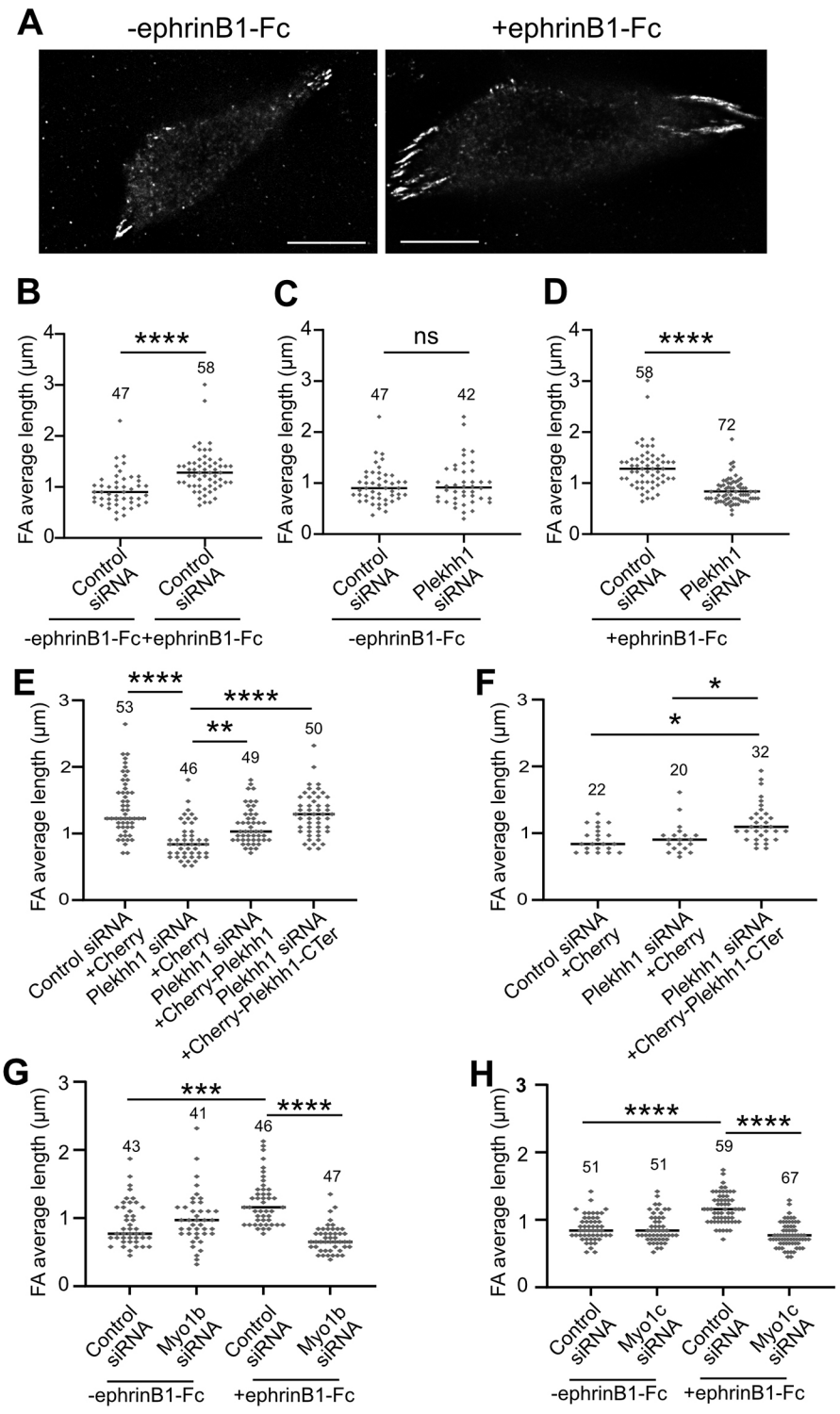

Fig. 7. Depletion of Plekhh1, Myo1b and Myo1c decreases the length of FAs in EphB2 stimulated cells. (A) Distribution of FAs in YFP–EphB2-HCT116 cells stimulated or not with ephrinB1–Fc. Cells were analysed by immunofluorescence with anti-vinculin antibodies and 3D deconvolution microscopy. Images represent a single focal plane at the base of the cells. Scale bars: 10 µm. (B) Scatter plots of FA average length per cell in YFP–EphB2-HCT116 cells stimulated or not with ephrinB1–Fc and treated with control siRNA. Data shown are the results of two experiments, with the median indicated (non-stimulated, *n*=47; stimulated, *n*=58). ****P<0.0001. (C) Scatter plots of FA average length per cell in non-stimulated YFP–EphB2-HCT116 cells treated with control or Plekhh1 siRNAs. Data shown are the results of two experiments, with the median indicated (control siRNA, *n*=47; Plekhh1 siRNA, *n*=42). ns, non-significant difference between the two different experimental conditions; P=0.9039. (D) Scatter plot of FA average length per cell in YFP–EphB2-HCT116 cells stimulated with ephrinB1–Fc and treated with control or Plekhh1 siRNAs. Data shown are the results of two experiments, with the median indicated (control siRNA, *n*=58; Plekhh1 siRNA, *n*=72). ****P<0.0001. (E) Scatter plot of FA average length per cell in YFP–EphB2-HCT116 cells stimulated with ephrinB1–Fc and co-transfected with control or Plekhh1 siRNAs and plasmids encoding mCherry, or siRNA-insensitive mCherry–Plekhh1 and mCherry–Plekhh1-CTer. Data shown are the results of two experiments, with the median indicated (control siRNA+mCherry, *n*=53; Plekkh1 siRNA+mCherry, *n*=46; Plekhh1 siRNA+mCherry–Plekhh1, *n*=49; Plekhh1 siRNA+mCherry–Plekhh1-CTer, *n*=50). ****P<0.0001; **P=0.0048. (F) Scatter plot of FA average length in non-stimulated YFP–EphB2-HCT116 cells co-transfected with control or Plekhh1 siRNAs and plasmids encoding mCherry or siRNA-insensitive mCherry–Plekhh1-CTer. Data shown are the results of a single experiment, with the median indicated (control siRNA+mCherry, *n*=22; Plekhh1 siRNA+mCherry, *n*=20; Plekhh1 siRNA+mCherry–Plekhh1-CTer, *n*=32). *P=0.0205 for control siRNA+mCherry and Plekhh1 siRNA+mCherry–Plekhh1-CTer, *P=0.0366 for Plekhh1 siRNA+mCherry and Plekhh1 siRNA+mCherry–Plekhh1-CTer. (G) Scatter plot of FA average length per cell, in YFP–EphB2-HCT116 cells stimulated or not with ephrinB1–Fc and treated with control or Myo1b siRNAs. Data shown are the results of two experiments, with the median indicated (non-stimulated control siRNA, *n*=43; non-stimulated Myo1b siRNA, *n*=41; stimulated control siRNA, *n*=46; stimulated, Myo1b siRNA, *n*=47). ***P=0.0001; ****P<0.0001. (H) Scatter plot of FA average length in YFP–EphB2-HCT116 cells stimulated or not with ephrinB1–Fc and treated with control or Myo1c siRNAs. Data shown are the results of two experiments, with the median indicated (non-stimulated control siRNA, *n*=51; non-stimulated Myo1c siRNA, *n*=51; stimulated control siRNA, *n*=59; stimulated Myo1c siRNA, *n*=67). ****P<0.0001. A non-parametric Mann–Whitney test (B–D) and non-parametric Kruskal–Wallis test followed by Dunn's multiple comparison test (E–H) were used for statistical testing.

pEGFP-C1 Plekhh1-NTer (amino acids 1–1617), pEGFP-C1 Plekhh1-CTer (amino acids 1618–4095), pEGFP-C1 MyTH-FERM (amino acids 2374–4095) and pEGFP-C1-FERM (amino acids 2911–4095) were generated with the same kit by cloning at EcoRI and SalI sites of pEGFP-C1 (Clontech) a DNA fragment generated by PCR of human Plekhh1 with 5′ primers 5′-gatctcgagctcaagcttcgaattctATGGCAGAACTCAAGGTGG-3′,

Journal of Cell Science (2021) 134, jcs258802. doi:10.1242/jcs.258802

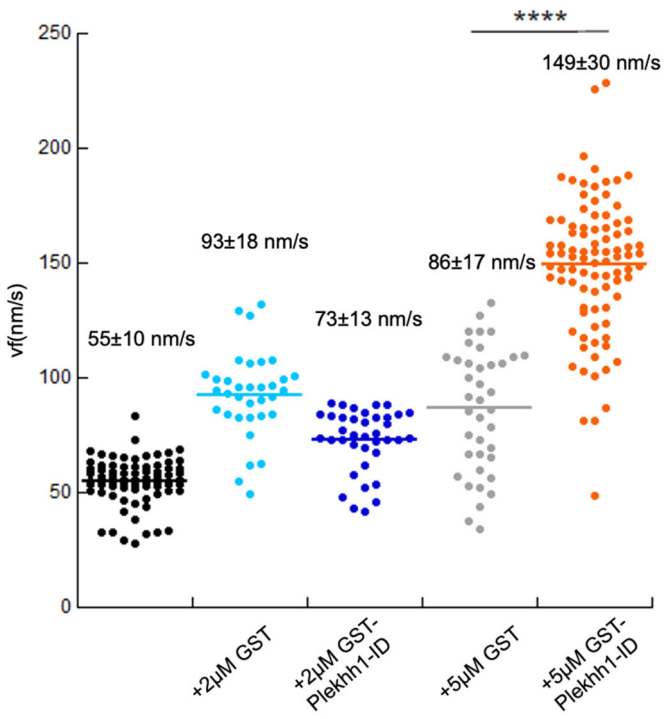

Fig. 8. The interacting domain of Plekhh1 increases Myo1b motor activity. Dot plot of the sliding velocity of stabilized F-actin (vf) in control conditions (black) and in the presence of the indicated concentrations of GST or GST–Plekhh1-ID. Sliding velocity was analysed from movies recorded using TIRF microscopy (see Materials and Methods). Mean±s.e.m. velocities are indicated on the graph (n=75 for control, 34 for GST 2 µM, 38 for GSTPlekhh1-ID 2 µM, 39 for GST 5 µM and 90 for GST-Plekhh1-ID 5 µM). ****P<0.0001 (Student's two-tailed unpaired t-test).

5′-gatctcgagctcaagcttcgaattctGACTACGCCATCCCCCCG-3′, 5′-gatctcgagctcaagcttcgaattctACAGTGGCTGCAGGTGGC-3′ and 5′-gatctcgagctcaagcttcgaattctGGGGAGCGGGAAGCCAGG-3′, respectively, and with 3′ primers 5′-atcccgggcccgcggtaccgtcgacTCAACCCTCGGAGCTCAG-3′ for Plekhh1-NTer and 5′-atcccgggcccgcggtaccgtcgacTCACAGCAACGTTGGCCC-3′ for the other constructs. pEGFP-C1 Plekhh1 was generated by subcloning Plekhh1 from pmCherry-C1 Plekhh1 at EcoRI and SalI sites. pmCherry Plekhh1-CTer was generated by subcloning the Plekhh1-CTer from pEGFP-C1 Plekhh1-CTer at EcoRI and SalI sites. GFP–Myo1b has been reported previously (Almeida et al., 2011). GFP–Myo1b motor and GFP–Myo1b-Tail were generated by cloning at EcoRI and XbaI or BglII and SalI sites of pEGFP-C1 (Clontech) DNA fragments generated by PCR on rat Myo1b iso b cDNA (NCBI accession number NM_053986) with 5′ primers 5′-atggccaagaaggaggtaaaat-3′ or 5′-attggccatcaagaccttaccta-3′ and 3′ primers 5′-ctgatatcgcttttgttgcgcgt-3′ or 5′-cctcacttaagggacagcgacttt-3′, respectively. GFP–Myo1b-IQ-Tail was obtained by deleting the fragment EcoRV-EcoRV from the recombinant plasmid encoding GFP–Myr 1 (Raposo et al., 1999). GFP–Myo1a, GFP–Myo1c and GFP–Myo6 (porcine isoform; UniProt F1RQI7) have been previously reported (Capmany et al., 2019; Loubéry et al., 2012; Waharte et al., 2005). Flag–EphB2 (pJK1), Flag–EphB2-KD (Lys660-Arg) (pJK2) and Flag–EphB2–YFP (pJK12) were a generous gift from Rudiger Klein (Max Planck, Martinsried, Germany) (Zimmer et al., 2003). mCherry–ephrinB1 was generated by PCR cloning of ephrinB1 from ECFP–HA–ephrinB1 (pJK30) (Zimmer et al., 2003) in the pmCherry-C1 plasmid

Cell culture, transfection and immunofluorescence labelling

HeLa and Hek293T cells were cultured at 37°C and 10% CO_2 in DMEM (Life Technologies, Carlsbad, CA, USA) supplemented with 10% fetal bovine serum (Eurobio, Courtaboeuf, France). YFP–EphB2-HCT116 and mCherry–ephrinB1-HCT116 cells have been previously isolated (Prospéri et al., 2015). For cell repulsion, 0.15×10^6 YFP–EphB2-HCT116 cells were co-cultivated with 0.15×10^6 mCherry–ephrinB1-HCT116 cells on glass-bottomed dishes (Fluorodish, World Precision Instruments, Sarasota, USA) coated with 0.05 mg/ml collagen [rat tail collagen I (354236, Corning)]. Cell repulsion was analysed using time-lapse microscopy 24 h after the beginning of the co-culture. For immunofluorescence labelling, YFP–EphB2-HCT116 cells were grown on glass coverslips coated with collagen (0.05 mg/ml; rat tail collagen I; Corning, NY, USA). For stimulation with ephrinB1–Fc, ephrinB1–Fc chimera (catalogue number 473EB; R&D Systems) was crosslinked with goat anti-human IgG Fc (2:1 ratio) and used at 5 µg/ml (Jackson ImmunoResearch). For recombinant protein expression, Hek293T or HeLa cells were transfected with cDNA using Effectene (Qiagen, Hilden, Germany), or Lipofectamine 3000 (Invitrogen), respectively, and were analysed 24 h later. For protein knockdown, YFP–EphB2-HCT116 cells were transfected with 50 nM, 10 nM or 12.5 nM of a non-targeting sequence (control siRNA; D-001810-01; Dharmacon, Lafayette, CO, USA), or 50 nM, 10 nM or 12.5 nM siRNAs targeting Plekhh1 (5′-CAGGAAGACCAGCGGACUA-3′; J-030302-10, Dharmacon), Myo1b (5′-GCUUACCUGGAAAUCAACAAG-3′; Almeida et al., 2011) and Myo1c (5′-GGGAGCCCGUCCAGUAUUU-3′; Sigma-Aldrich), respectively, using Lipofectamine RNAiMax (Invitrogen). Cells were analysed after 48 h or after 72 h for rescue experiments (Figs 6B,D and 7E). For immunofluorescence labelling, cells were fixed with 3% paraformaldehyde and permeabilized with 0.1% Triton X-100 or 0.1% saponin before antibody incubation using a standard procedure (Prospéri et al., 2015).

Purification of GST-tagged recombinant proteins

An 0.8 (600 nm) optical density culture of *E. coli* transformed with the GST plasmids – GST, GST–Plekhh1-ID or GST–Plekhh1(53–597) – was grown in a shaker at 37°C. After removing an aliquot before IPTG treatment (1/25th of the culture), 1 mM IPTG (Euromedex, Souffelweyersheim, France) was added for 30 min. The aliquots and the cultures were centrifuged at 6000 ***g*** for 20 min at 4°C, and the aliquot and culture pellets were resuspended with 1 ml or 25 ml, respectively, of cold phosphate-buffered saline (PBS) containing 0.1% protease inhibitor cocktail (PIC; Sigma-Aldrich), sonicated (twice for 2 min, 30% amplitude), adjusted to 1% Triton X-100 and agitated for 30 min at 4°C. After centrifugation at 15,000 ***g*** for 20 min at 4°C, 100 µl of the supernatant was adjusted with Laemmli buffer supplemented with β-mercaptoethanol and boiled 5 min before analysis on SDS–PAGE and Coomassie Blue staining to test the expression of the recombinant proteins depending on the IPTG treatment. Then, 1 ml of glutathione sepharose beads (GE Healthcare, Chicago, IL, USA) was added to the supernatant and agitated overnight at 4°C. After centrifugation at 500 ***g*** for 5 min at 4°C, the beads were washed once with PBS, 0.1% PIC and 0.1% Triton X-100 at room temperature and twice with PBS and 0.1% PIC. Then, the beads were resuspended 2X in 1 ml of Elution Buffer (20 mM glutathione, 50 mM Tris-HCl pH 8, 150 mM NaCl and 0.1% PIC) and mixed for 2 h at 4°C. For purification of anti-Plekhh1 antibodies, a dialysis overnight in 0.2 M $NaHCO_3$ and 0.5 M NaCl was performed, and the recombinant GST–Plekhh1 (amino acids 53–597) was loaded on a HiTrap NHS-activated column (GE Healthcare). For the motility assay, a dialysis overnight of GST or GST–Plekhh1-ID in 50 mM Tris-HCl pH 7.4, 1 mM EDTA and 0.15 M NaCl was performed, and the proteins were aliquoted and kept at −80°C. For GST pull-down experiments, the beads loaded with GST or GST–Plekhh1-ID were directly used in the experiment.

Mouse tissue extracts

Organs from C57BL/6N mice (Charles River Wilmington, Massachssetts USA) were crushed in Potter homogenizers in 500 µl of Laemmli buffer supplemented with 100 mM DTT and 0.5% PIC (Sigma-Aldrich), then incubated for 20 min at room temperature and directly boiled for 5 min for brain, spleen and ileum. The supernatant was collected after 10 min of centrifugation at 12,000 ***g*** and boiled for 5 min for colon, kidney, liver and lung. All extracts were sonicated for 30 s in ice, and supernatants were collected after centrifugation at 20,000 ***g*** for 15 min for spleen, ileum, colon, liver and lung or for 30 min for brain and kidney. The resulting supernatants were then boiled for 3 min. Protein concentration of organ extracts was estimated by loading 2 µl, 5 µl and 10 µl of concentrated (1/2 dilution) or

diluted (1/10 dilution) samples of each extract on SDS–PAGE gels that were subsequently stained with Coomassie Blue. Then, equal amounts of proteins were loaded on SDS-PAGE gels for immunoblotting. All animal experiments were performed according to approved guidelines.

GST pull down and GFP-Trap

6×10^6 cells were incubated for 30 min on ice in 1 ml lysis buffer containing 50 mM Tris-HCl pH 7.4, 150 mM NaCl, 1% Triton X-100, 1 mM EDTA, 1 mM EGTA, 10 mM ATP (for cells expressing myosins), 10% glycerol, 1 mM DTT, 0.1% PIC, and 0.15 mM sodium orthovanadate and 1% phosphatase inhibitor cocktail (Sigma-Aldrich) (for cells expressing Flag–EphB2). After 20 min of centrifugation of the cell lysates at 20,000 ***g***, 1 ml of supernatant was incubated for 2 h at 4°C with 26 µg of GST or GST–Plekhh1-ID loaded on glutathione sepharose beads for GST pull-down or incubated overnight at 4°C with 25 µl of GFP-Trap beads (Chromotek, Planegg, Martinsried, Germany) for GFP-Trap experiments. Then, beads were washed five times with lysis buffer, resuspended in 25 µl of Laemmli buffer supplemented with β-mercaptoethanol and boiled for 5 min before analysis by immunoblotting.

Immunoblotting

Proteins separated by SDS–PAGE were transferred to nitrocellulose membranes and processed for immunoblotting using Super Signal West Pico Chemiluminescent substrate (Thermo Fisher Scientific, Waltham, MA, USA) or Lumilight Western Blotting Substrate (Roche). Images of immunoblots were captured with Chemidoc Touch Biorad 2 or with CL-XPosure Film (Thermo Fisher Scientific) within the linear range and quantified by densitometry using the 'analyze gels' function in ImageJ (https://imagej.nih.gov/ij/).

Single-filament TIRF microscopy assays

Actin and Myo1b were purified as described previously (Pernier et al., 2020). The flow chamber was prepared as described by Pernier and colleagues (Pernier et al., 2020). The chamber was incubated with 100 nM anti-Myo1b antibody in G buffer (5 mM Tris-HCl, pH 7.8, 0.1 mM $CaCl_2$, 0.2 mM ATP, 1 mM DTT and 0.01% NaN_3) for 10 min at room temperature. The chamber was rinsed three times with G buffer, 0.1% BSA and incubated for 5 min at room temperature. Then the chamber was incubated with 300 nM Alexa Fluor 488-labelled Myo1b in Fluo F buffer (5 mM Tris-HCl, pH 7.8, 100 mM KCl, 1 mM $MgCl_2$, 0.2 mM EGTA, 2 mM ATP, 10 mM DTT, 1 mM DABCO and 0.01% NaN3) and 50 µM calmodulin for 10 min at room temperature. Assays were performed in Fluo F buffer, containing 2 mM constant ATP, supplemented with 0.3% methylcellulose (Sigma-Aldrich), 20 nM actin filaments (stabilized with phalloidin–Alexa Fluor 547) and in the absence or presence of GST–Plekhh1-ID (5 µM). To maintain constant concentration of ATP in this assay an ATP regenerating mix, including 2 mM ATP, 2 mM $MgCl_2$, 10 mM creatine phosphate and 3.5 U/ml creatine phosphokinase, was added. The sliding of actin filaments on Myo1b was monitored by TIRF microscopy (Eclipse Ti inverted microscope, 100× TIRF objectives, Quantem 512SC camera). The experiments were controlled using Metamorph software (Molecular Devices). The velocity of single filaments was analysed with the Kymo Tool Box plugin of Image J software (https://github.com/fabricecordelieres/IJ_KymoToolBox). Only filaments longer than 20 pixels and moving directionally during the whole sequence were selected. On each image of a sequence, a segmented line was manually drawn over a single filament to generate a 10-pixel-wide band. The plugin flattens the curved filaments and generates a kymograph. The accuracy of the displacement and the length of the filaments is of the order of the pixel size (160 nm). We consider that each actin subunit contributes to 2.7 nm of the filament length.

Image acquisition

Image acquisition and image analysis were performed on workstations of the PICT-IBiSA Lhomond Imaging facility of Institut Curie. Epifluorescence microscopy (Fig. 2; Figs S2 and S5) was carried out with a Leica DM6B microscope equipped with 100× NA 1.4 oil immersion objective and a sCMOS camera (Orca Flash 4.0 V2; Hamamatsu, Japan). Three-dimensional (3D) deconvolution microscopy (Figs 5A and 7A) was carried out using an Upright Nikon Ni-E microscope equipped with a 100× NA 1.4 oil immersion objective, a piezo-electric driver mounted underneath the objective and a CoolSNAP HQ2 camera. *Z* series of images were taken at 0.2 µm increments. Deconvolution was carried out by the 3D deconvolution Metamorph module with the fast iterative constrained PSF-based algorithm44. Spinning-disc confocal microscopy (Fig. 3A; Movie 1) was carried out with a Yokogawa CSU-X1 on a Nikon Inverted Eclipse TI-E microscope equipped with a 40× NA 1.3 oil immersion objective and a sCMOS Prime 95B (Photometrics) camera under 5% CO_2 and at 37°C. Spinning-disc confocal microscopy (Fig. 5B; Movies 2,3) was carried out with a Yokogawa CSU-X1 on a Nikon Inverted Eclipse TI-E microscope equipped with super resolution module – Live-SR (Gataca Systems) – with a 100× NA 1.4 oil immersion objective. 3D reconstructions were generated by using the software Fiji (https://fiji.sc/).

Statistical analysis

To avoid neighbouring cells affecting the behaviour of the analysed cells, we considered only isolated cells on the coverslips. For comparison of two conditions (Fig. 7B–D) a non-parametric Mann–Whitney test was performed using GraphPad Prism version 9.0.0 for Windows (GraphPad Software, San Diego, CA, USA; www.graphpad.com). For comparison of four conditions (Fig. 6A,B and Fig. 7E–H) a non-parametric Kruskal–Wallis test followed by Dunn's multiple comparison was performed with GraphPad Prism. For experiments with percentage comparison (Fig. 3C and Fig. 6C–F) a Fisher's exact test, with Benjamini–Hochberg multiple comparison correction applied when necessary, was performed with R version 3.5.2 (R Core Team, 2020). For western blots, a two-tailed unpaired *t*-test with Welch's correction was performed using GraphPad Prism (Fig. 1G,I and Fig. 4C,D,F,G; Fig. S1). Statistical analysis in Fig. 8 was performed by using a Student's two-tailed unpaired *t*-test with Microsoft Excel.

Empirical cumulative density function

In order to give the same statistical weight to each cell for the analysis of the distribution of FA length, we computed empirical cumulative density functions (ECDFs) for FA length as follows: an ECDF was computed for each cell, and then we computed an average ECDF curve for a given condition. Each ECDF curve has an envelope that represents the s.e.m. To test whether the cells followed the same distribution of FA length, we used the two-sample Cramér–von Mises criterion (Anderson, 1962). However, the analytical expression of the distribution of Cramér–von Mises criterion under the null hypothesis is unknown (for large samples). Therefore, we used a permutation test to evaluate the significance. We made 1000 permutations (drawn randomly among all possible permutations without replacement) to evaluate the exact distribution of the Cramér–von Mises criterion. Note, we permutated cells (i.e. group of FAs) and not individual FAs. A Benjamini–Hochberg procedure was used to correct multiple comparisons. The statistical analysis was performed using R version 3.5.2 (R Core Team, 2020).

Acknowledgements

We thank A. Gaudreau (Ecole polytechnique, Palaiseau, France) for providing modified pGEX-CS2, and K. Schauer (Institut Curie, Paris, France) for providing Myo1c constructs. The authors greatly acknowledge Cell and Tissue Imaging (PICT-IBiSA), Institute Curie, which is a member of the French National Research Infrastructure France – Bioimaging (ANR-10-IBNS-04).

Competing interests

The authors declare no competing or financial interests.

Author contributions

Conceptualization: E.C.; Methodology: M.-T.P., J.P., H.L.; Formal analysis: M.-T.P., J.P., H.L.; Investigation: M.-T.P., J.P.; Writing - original draft: M.-T.P., E.C.; Writing - review & editing: E.C.; Supervision: E.C.; Project administration: E.C.; Funding acquisition: E.C.

Funding

This work was supported by Institut Curie, Centre National de la Recherche Scientifique (CNRS), the Agence Nationale de la Recherche (ANR-14-CE11-0005-01)

and the European Research Council (project 339847). The E.C. laboratory is a member of the CNRS consortium CellTiss, the Labex CelTisPhyBio (Agence Nationale de la Recherche, ANR-11-LABX0038) and Paris Sciences et Lettres (Agence Nationale de la Recherche, ANR-10-IDEX-0001-02).

References

Aguilar-Cuenca, R., Juanes-García, A. and Vicente-Manzanares, M. (2014). Myosin II in mechanotransduction: master and commander of cell migration, morphogenesis, and cancer. *Cell Mol. Life Sci.* **71**, 479-492. doi:10.1007/s00018-013-1439-5

Almeida, C. G., Yamada, A., Tenza, D., Louvard, D., Raposo, G. and Coudrier, E. (2011). Myosin 1b promotes the formation of post-Golgi carriers by regulating actin assembly and membrane remodelling at the trans-Golgi network. *Nat. Cell. Biol.* **13**, 779-789. doi:10.1038/ncb2262

Anderson, T. W. (1962). On the distribution of the two-sample Cramer-von Mises criterion. *Ann. Math. Statist.* **33**, 1148-1159. doi:10.1214/aoms/1177704477

Batlle, E. and Wilkinson, D. G. (2012). Molecular mechanisms of cell segregation and boundary formation in development and tumorigenesis. *Cold Spring Harb. Perspect. Biol.* **4**, a008227. doi:10.1101/cshperspect.a008227

Batlle, E., Henderson, J. T., Beghtel, H., van den Born, M. M. W., Sancho, E., Huls, G., Meeldijk, J., Robertson, J., van de Wetering, M., Pawson, T. et al. (2002). Cell Beta-catenin and TCF mediate cell positioning in the intestinal epithelium by controlling the expression of EphB/ephrinB. *Cell.* **111**, 251-263. doi:10.1016/S0092-8674(02)01015-2

Capmany, A., Yoshimura, A., Kerdous, R., Caorsi, V., Lescure, A., Del Nery, E., Coudrier, E., Goud, B. and Schauer, K. (2019). MYO1C stabilizes actin and facilitates the arrival of transport carriers at the Golgi complex. *J. Cell Sci.* **132**, jcs225029. doi:10.1242/jcs.225029

Fagotto, F., Rohani, N., Touret, A.-S. and Li, R. (2013). A molecular base for cell sorting at embryonic boundaries: contact inhibition of cadherin adhesion by ephrin/ Eph-dependent contractility. *Dev. Cell.* **27**, 72-87. doi:10.1016/j.devcel.2013.09.004

Groeger, G. and Nobes, C. D. (2007). Co-operative Cdc42 and Rho signalling mediates ephrinB-triggered endothelial cell retraction. *Biochem. J.* **404**, 23-29. doi:10.1042/BJ20070146

Gupta, P., Gauthier, N. C., Cheng-Han, Y., Zuanning, Y., Pontes, B., Ohmstede, M., Martin, R., Knolker, H. J., Dobereiner, H. G., Krendel, M. et al. (2013). Myosin 1E localizes to actin polymerization sites in lamellipodia, affecting actin dynamics and adhesion formation. *Biol. Open.* **2**, 1288-1299. doi:10.1242/bio.20135827

Huang, X., Cheng, H.-J., Tessier-Lavigne, M. and Jin, Y. (2002). MAX-1, a novel PH/MyTH4/FERM domain cytoplasmic protein implicated in netrin-mediated axon repulsion. *Neuron* **34**, 563-576. doi:10.1016/S0896-6273(02)00672-4

Iuliano, O., Yoshimura, A., Prosperi, M. T., Martin, R., Knolker, H. J. and Coudrier, E. (2018). Myosin 1b promotes axon formation by regulating actin wave propagation and growth cone dynamics. *J.Cell Biol.* **217**, 2033-2046.

Joensuu, M., Belevich, I., Rämö, O., Nevzorov, I., Vihinen, H., Puhka, M., Witkos, T. M., Lowe, M., Vartiainen, M. K. and Jokitalo, E. (2014). ER sheet persistence is coupled to myosin 1c-regulated dynamic actin filament arrays. *Mol. Biol. Cell.* **25**, 1111-1126. doi:10.1091/mbc.e13-12-0712

Kayser, M. S., Nolt, M. J. and Dalva, M. B. (2008). EphB receptors couple dendritic filopodia motility to synapse formation. *Neuron.* **59**, 56-69. doi:10.1016/j.neuron.2008.05.007

Kindberg, A. A., Srivastava, V., Muncie, J. M., Weaver, V. M., Gartner, Z. J. and Bush, J. O. (2021). EPH/EPHRIN regulates cellular organization by actomyosin contractility effects on cell contacts. *J.Cell Biol.* **220**, e202005216. doi:10.1083/jcb.202005216

Klein, R. (2012). Eph/ephrin signalling during development. *Development.* **139**, 4105-4109. doi:10.1242/dev.074997

Laakso, J. M., Lewis, J. H., Shuman, H. and Ostap, E. M. (2010). Control of myosin-I force sensing by alternative splicing. *Proc. Natl. Acad. Sci. USA* **107**, 698-702. doi:10.1073/pnas.0911426107

Loubéry, S., Delevoye, C., Louvard, D., Raposo, G. and Coudrier, E. (2012). Myosin VI regulates actin dynamics and melanosome biogenesis. *Traffic* **13**, 665-680. doi:10.1111/j.1600-0854.2012.01342.x

Marston, D. J., Dickinson, S. and Nobes, C. D. (2003). Rac-dependent trans-endocytosis of ephrinBs regulates Eph-ephrin contact repulsion. *Nat. Cell Biol.* **5**, 879-888. doi:10.1038/ncb1044

McIntosh, B. B. and Ostap, E. M. (2016). Myosin-I molecular motors at a glance. *J. Cell Sci.* **129**, 2689-2695. doi:10.1242/jcs.186403

Moeller, M. L., Shi, Y., Reichardt, L. F. and Ethell, I. M. (2006). EphB receptors regulate dendritic spine morphogenesis through the recruitment/phosphorylation of focal adhesion kinase and RhoA activation. *J. Biol. Chem.* **281**, 1587-1598. doi:10.1074/jbc.M511756200

O'Neill, A. K., Kindberg, A. A., Niethamer, T. K., Larson, A. R., Ho, H.-Y. H., Greenberg, M. E. and Bush, J. O. (2016). Unidirectional Eph/ephrin signaling creates a cortical actomyosin differential to drive cell segregation. *J. Cell Biol.* **215**, 217-229. doi:10.1083/jcb.201604097

Percipalle, P. and Farrants, A.-K. (2006). Chromatin remodelling and transcription: be-WICHed by nuclear myosin 1. *Curr. Opin. Cell Biol.* **18**, 267-274. doi:10.1016/j.ceb.2006.03.001

Perisic, L., Lal, M., Hulkko, J., Hultenby, K., Önfelt, B., Sun, Y., Dunér, F., Patrakka, J., Betsholtz, C., Uhlen, M. et al. (2012). Plekhh2, a novel podocyte protein downregulated in human focal segmental glomerulosclerosis, is involved in matrix adhesion and actin dynamics. *Kidney Int.* **82**, 1071-1083. doi:10.1038/ki.2012.252

Pernier, J., Kusters, R., Bousquet, H., Lagny, T., Morchain, A., Joanny, J.-F., Bassereau, P. and Coudrier, E. (2019). Myosin 1b is an actin depolymerase. *Nat. Commun.* **10**, 5200. doi:10.1038/s41467-019-13160-y

Pernier, J., Morchain, A., Caorsi, V., Bertin, A., Bousquet, H., Bassereau, P. and Coudrier, E. (2020). Myosin 1b flattens and prunes branched actin filaments. *J. Cell Sci.* **133**, jcs247403. doi:10.1242/jcs.247403

Prospéri, M.-T., Lépine, P., Dingli, F., Paul-Gilloteaux, P., Martin, R., Loew, D., Knölker, H.-J. and Coudrier, E. (2015). Myosin 1b functions as an effector of EphB signaling to control cell repulsion. *J. Cell Biol.* **210**, 347-361. doi:10.1083/jcb.201501018

R Core Team. (2020). *R: A Language and Environment for Statistical Computing*. Vienna, Austria: R foundation for statistical computing. https://www.R-project.org/.

Raposo, G., Cordonnier, M.-N., Tenza, D., Menichi, B., Dürrbach, A., Louvard, D. and Coudrier, E. (1999). Association of myosin I alpha with endosomes and lysosomes in mammalian cells. *Mol. Biol. Cell.* **10**, 1477-1494. doi:10.1091/mbc.10.5.1477

Rohani, N., Canty, L., Luu, O., Fagotto, F. and Winklbauer, R. (2011). EphrinB/EphB signaling controls embryonic germ layer separation by contact-induced cell detachment. *PLoS Biol.* **9**, e1000597. doi:10.1371/journal.pbio.1000597

Sackmann, E. (2015). How actin/myosin crosstalks guide the adhesion, locomotion and polarization of cells. *Biochim. Biophys. Acta.* **1853**, 3132-3142. doi:10.1016/j.bbamcr.2015.06.012

Salas-Cortes, L., Ye, F., Tenza, D., Wilhelm, C., Theos, A., Louvard, D., Raposo, G. and Coudrier, E. (2005). Myosin Ib modulates the morphology and the protein transport within multi-vesicular sorting endosomes. *J. Cell Sci.* **118**, 4823-4832. doi:10.1242/jcs.02607

Schaks, M., Giannone, G. and Rottner, K. (2019). Actin dynamics in cell migration. *Essays Biochem.* **63**, 483-495. doi:10.1042/EBC20190015

Waharte, F., Brown, C. M., Coscoy, S., Coudrier, E. and Amblard, F. (2005). A two-photon FRAP analysis of the cytoskeleton dynamics in the microvilli of intestinal cells. *Biophys. J.* **88**, 1467-1478. doi:10.1529/biophysj.104.049619

Zhong, H., Wu, X., Huang, H., Fan, Q., Zhu, Z. and Lin, S. (2006). Vertebrate MAX-1 is required for vascular patterning in zebrafish. *Proc. Natl. Acad. Sci. U S A.* **103**, 16800-16805. doi:10.1073/pnas.0603959103

Zimmer, M., Palmer, A., Köhler, J. and Klein, R. (2003). EphB-ephrinB bi-directional endocytosis terminates adhesion allowing contact mediated repulsion. *Nat. Cell Biol.* **5**, 869-878. doi:10.1038/ncb1045